IAS SEDIMENTOLOGY
Journal of the International Association of Sedimentologists

Pyroclastic dune bedforms: macroscale structures and lateral variations. Examples from the 2006 pyroclastic currents at Tungurahua (Ecuador).

Journal:	*Sedimentology*
Manuscript ID	SED-2018-OM-150.R1
Manuscript Type:	Original Manuscript
Date Submitted by the Author:	n/a
Complete List of Authors:	Douillet, Guilhem; Universität Bern, Institut für Geologie; Ludwig-Maximilians-Universität, Department für Geo und Umweltwissenschaften Bernard, Benjamin; Escuela Politecnica Nacional Instituto Geofisico Bouysson, Mélanie; Universite de Strasbourg Ecole et Observatoire des Sciences de la Terre, EOST Chaffaut, Quentin; Universite de Strasbourg Ecole et Observatoire des Sciences de la Terre Dingwell, Donald; Ludwig-Maximilians-Universität, Department für Geo und Umweltwissenschaften Gegg, Lukas; Universität Bern, Institut für Geologie Hoelscher, Inga; Ludwig-Maximilians-Universität, Department für Geo und Umweltwissenschaften Kueppers, Ulrich; Ludwig-Maximilians-Universität, Department für Geo und Umweltwissenschaften Mato, Célia; Universite Grenoble Alpes Ritz, Vanille; eidgenossische Technische Hochschule, Swiss Seismological Survey, Swiss Seismological Survey Schlunegger, Fritz; University of Bern, Institute of Geological Sciences Witting, Patrick; Ludwig-Maximilians-Universität, Department für Geo und Umweltwissenschaften
Keywords:	Backset lamination, Dune bedforms, Pyroclastic currents, Stoss-aggradation, Tungurahua

Pyroclastic dune bedforms: macroscale structures and lateral variations. Examples from the 2006 pyroclastic currents at Tungurahua (Ecuador).

Guilhem Amin Douillet[1,2], Bernard B.[3], Bouysson M.[2,4], Chaffaut Q.[2,4], Dingwell D.B.[2], Gegg L.[1,2], Hoelscher I.[2], Kueppers U.[2], Mato C.[5], Ritz V.A.[6], Schlunegger F.[1], Witting P.[2]

1: Institut für Geologie, Universität Bern, Switzerland
2: Earth and Environmental Sciences. Ludwig-Maximilians-Universität München, Germany
3: Instituto Geofisico, Escuela Politécnica Nacional, Quito, Ecuador
4: Ecole Et Observatoire des Sciences de la Terre, Université de Strasbourg, France
5: Université Joseph Fourier Grenoble, France
6: Swiss Seismological Service, Eidgenössische Technische Hochschule Zürich, Switzerland

Abstract

Pyroclastic currents are catastrophic flows of gas and particles triggered by explosive volcanic eruptions. For much of their dynamics, they behave as particulate density currents and share similarities with turbidity currents. They occasionally deposit dune bedforms with peculiar lamination patterns, from what is thought to represent the dilute, low concentration, and fluid-turbulence supported end member of the pyroclastic currents. Here, we present a high resolution dataset of sediment plates (lacquer peels) with several closely spaced lateral profiles representing sections through single pyroclastic bedforms from the August 2006 eruption of Tungurahua (Ecuador).

Most of the sedimentary features contain backset bedding and preferential stoss-face deposition. From the ripple scale (few cm) to the largest dune bedform scale (several m length), similar patterns of erosive-based backset beds are evidenced. Recurrent trains of sub-vertical truncations on the stoss side of structures reshape and steepen the bedforms. In contrast, sporadic coarse-grained lenses and lensoidal layers flatten bedforms by filling troughs. The coarsest (clasts up to 10 cm), least sorted and massive structures still exhibit lineation patterns that follow the general backset bedding trend. The stratal architecture exhibits strong lateral variations within tens of centimeters, with very local truncations both in flow-perpendicular and flow-parallel direction.

We infer that the bedforms' sedimentary patterns result from four formation mechanisms: "differential draping", "slope-influenced saltation", "truncative bursts", and "granular-based events". Whereas most of the literature makes a straightforward link between backset bedding and Froude-supercritical flows, we reconsider this interpretation. Indeed, features that would be diagnostic of subcritical dunes, antidunes, and "chute and pools" can be found on the same horizon and in a single bedform, only laterally separated by short distances (10s of cm). Our data stress the influence of the pulsating and highly turbulent nature of the currents and the possible role of coherent flow structures such as Görtler vortices. Backset bedding is interpreted here as a consequence of a very high sedimentation environment of weak and waning currents that interact with the pre-existing morphology.

Quantification of near-bed flow velocities are made via comparison with wind tunnel experiments. We estimate that shear velocities of ca. 0.30 $m.s^{-1}$ (equivalent to pure wind velocity of 6 to 8 $m.s^{-1}$ at 10 cm above the bed) could emplace the constructive bedsets, whereas the truncative phases would result from bursts with impacting wind velocities of at least 30-40 $m.s^{-1}$.

Keywords: Backset lamination, Dune bedforms, Pyroclastic currents, Tungurahua, stoss-aggradation

Running title: Pyroclastic dune bedforms from the 2006 pyroclastic currents at Tungurahua

1. Introduction

1.1. Turbulent pyroclastic currents

Pyroclastic currents are ground-hugging gas-pyroclast mixtures whose flow is generally driven by gravity and triggered by volcanic eruptions (Dufek 2016, Sulpizio et al. 2014, Palladino 2017). A range of flow processes, ranging from concentrated granular flows dominated by particle-particle interactions, to fluidized mixtures and up to fully turbulent, fluid-supported currents is interpreted from the study of deposits (e.g. Fisher 1990, Cole and Scarpati 1993, Branney and Kokelaar 2002, Douillet et al. 2013a, Sulpizio et al. 2014). The flow-bed boundary layer is the coupling element between the flow structure and the bed morphology, being influenced by and influencing both the flow and the bed (Branney and Kokelaar 1992, 2002, Dellino et al. 2004a, Douillet et al. 2013a, Breard et al. 2016). The processes acting at this flow-bed boundary layer have a crucial influence on the grain size distribution, the texture or fabric, and depositional patterns of the sediment (Branney and Kokelaar 2002). Deposits containing fine-scale laminasets forming dune bedforms have been interpreted as resulting from the low-concentration, turbulence-dominated, end-member of pyroclastic currents (e.g. Sparks and Walker 1973, Cole 1990, Druitt 1992, Dellino et al. 2004b - commented by Le Roux 2005-, Douillet et al. 2013b). Such "dilute pyroclastic currents" may result from decreased density resulting from thermal expansion of entrained air (Andrews 2014), flow stripping at cliffs (Douillet et al. 2013a), or may be related to the initial eruptive dynamics, in particular for highly explosive maar volcanoes (e.g. Waters and Fisher 1971, Jordan et al. 2013). They are envisioned as behaving as a particular type of particulate density currents, i.e. a flow with gravity as driving force, and where turbulently suspended particles, that ultimately sediment to form deposits, are the agent of excess density driving the flow (Simpson 1982). As such, dilute pyroclastic currents are likely to be related to subaqueous turbidity currents, and a comparison of their dynamics and sedimentary signature is therefore highly relevant (Branney and Kokelaar 1992, Kneller and Buckee 2000). A smooth continuum between the granular and turbulent end-member flow behaviors is often modeled and expected in nature (Breard et al. 2016, Burgisser and Bergantz 2002)

1.2. The stoss-aggrading nature of pyroclastic bedforms

Dune bedforms emplaced by pyroclastic currents are notorious for their stoss-aggrading nature producing a variety of backset laminations (e.g. Schmincke et al. 1973, Cole 1991, Douillet et al. 2013b and references therein). Early authors have suggested that these characteristics could link to the interpretation as Froude-supercritical bedforms (Fisher and Waters 1969, 1970; Waters and Fisher 1971, Crowe and Fisher 1973, Mattson and Alvarez 1973, Schmincke et al. 1973). Subsequently, this stoss-aggrading characteristic of the deposits has largely been taken as a straightforward argument for parental Froude-supercritical flows without further debate (Fisher 1977, Yokoyama and Tokunaga 1978, Wohletz and Sheridan 1979, Walker et al. 1981, Fisher et al. 1983, Suthren 1985, Sohn and Chough 1989, Charland and Lajoie 1989, Gianneti and Luongo 1994, Brand and White 2007, Gençalioğlu-Kuşcu et al. 2007, Kelfoun et al. 2009, Brand et al. 2009, Brand and Clarke 2009, 2012). Froude-supercritical flows are defined as flows with more energy stored as kinetic energy than (gravity) potential energy (and thus the dimensionless Froude number expressing this ratio is above 1, e.g. Kennedy, 1963, Cartigny et al. 2011, 2014, Douillet 2015 - Chapter 2). When the ambient fluid's density is non-negligible in comparison to the density of the flow, the expression of the Froude number appears as the densiometric Froude number. Although Froude-supercritical flows are mostly known for their upstream aggrading (backset bedding) and upper plane beds signature, they can also produce laminations that aggrade downstream (e.g. Spinewine et al. 2009). The direct link between backset laminations and Froude-supercritical bedforms has been questioned in the pyroclastic context as well as for turbidites (e.g. Kubo and Nakajima 2002, Douillet et al. 2013b) and alternative interpretations have been suggested. In particular, the differential draping of a fallout load in a weak current was suggested to explain the processes of "regressive climbing dunes" for pyroclastic bedforms (Douillet et al. 2013b), following a similar interpretation for turbidity currents (Ponce and Carmona 2011). Recently, Vellinga et al. (2018) showed that for analogue and numerical experimental

currents, preferential stoss-aggradation occurs downstream of a hydraulic jump, in the subcritical regions dominated by slow, vertically-expanding current.

The role of topography

The possibility of stoss-aggradation being forced by the inherited bed topography was put forward for turbidity currents (Nakajima and Satoh 2001, Kubo and Nakajima 2002). In the pyroclastic context, it was suggested that the shape of a bedform alone could force saltating particles to deposit preferentially on stoss-faces in a feedback effect (Douillet et al. 2014). Indeed, the saltation threshold (the minimum shear required from a current to put particles in saltation) was measured for pyroclastic particles at various bed-slopes and found to be 50% higher on stoss- vs. lee-faces (Douillet et al. 2014). The role of bed-slope has been further emphasized in the type of pyroclastic bedform produced, with evidences that dune bedforms are more likely to develop when the flow climbs up a ridge (Breard et al. 2015), that stoss-deposition is more frequent when flows climbed up-ridge than flowing down (Druitt 1992) and that giant regressive bedforms resulted from a dual bypass upstream and downstream from a depositional zone of backset beds (Brown and Branney 2004). Pyroclastic bedforms continuing their growth over several pulses or flows (e.g. Walker 1984, Cole 1991, Sulpizio et al. 2007), the interaction of the subsequent flow with the pre-existing topography can have a dominant role in sedimentation. Apart from Druitt (1992), no studies have yet addressed lateral variations within single pyroclastic bedforms, or the retro-controls of a developing bedform on its subsequent growth.

1.3. Erosional structures from turbulent pyroclastic currents

Since the recognition of the primary nature of pyroclastic dune bedforms, most documented outcrops included steep truncations of their stoss faces, generally called "chute-and-pools" and interpreted as representing the signature of hydraulic jumps (called here Froude-jumps, i.e. a jump of the Froude regime from supercritical to subcritical) in some basal layer of the flow (e.g. Schmincke et al. 1973, Gençalioğlu-Kuşcu et al. 2007; Brand et al 2009). Recently, most characteristics of such stoss-side truncations, in particular their abrupt and steep termination, could be reproduced using experimental short-lived air bursts unrelated to a jump in flow regime (Douillet et al. 2017).

Under water, scours caused by wall jets have been the focus of extensive work in the engineering context (e.g. Balachandar and Reddy 2013). Interestingly, Dumas et al. (2005) noted that experimental bedforms created under combined flows had a “boxy profile” when stoss faces were steepened by intense local scouring.

Besides these truncated bedforms, erosional, longitudinal U-shaped channels formed during the flow of pyroclastic currents have intrigued volcanologists for decades. Richards (1959) documented large-scale, parallel furrows that covered the upper flanks of Barcena volcano (Mexico) briefly after the 1952 eruption. Those furrows terminated abruptly at change of slope, and large boulders were sometimes present at their upstream initiation. Similar features were reported by Kieffer and Sturtevant (1988) from the 1980 Mt. St. Helens eruption (Washington, USA). They were present in zones of flow reattachment downstream of sheltered regions and were attributed to scouring by longitudinal vortices resulting from flow instabilities induced by topography. Fisher (1977) also documented U-shaped (and V-shaped) channels in stratified pyroclastic deposits, interpreted as erosion from "base surges". He suggested that a flow front would develop a "cleft and lobe pattern", with "lobes being individual turbulent cells that splay outward from the source". Thus most interpretations involve coherent structures related to a flow's turbulence.

Here, we document the sedimentary information found in pyroclastic dune bedforms at the lamina scale and through a survey of closely-spaced lateral transects. We show that single bedforms drastically vary in their aggrading nature, and suggest three processes of stoss-deposition unrelated to Froude-supercritical flows, which enable estimations of near-bed velocities of the parental currents.

2. The Tungurahua set of sediment plates

2.1. Context of the deposits of the 2006 eruption of Tungurahua

The dataset presented here was created from the unconsolidated deposits of the pyroclastic currents triggered during the 17 August 2006 explosive eruption of Tungurahua volcano (Ecuador). These pyroclastic currents deposited two end member sedimentary facies as a consequence of their interaction with the ravines on the steep flanks of the volcano. The valley-bottom facies is dominated by coarse grained, (up to metric size boulders), unsorted, massive layers (1-5 m thick, Kelfoun et al. 2009, Douillet et al. 2013a, Hall et al. 2013). The marginal facies occurs outside curves of valleys, on shoulders and overbanks, and forms individual patches of a few 100s of meters in extent consisting of fields of meter-size dune bedforms (Douillet et al. 2013b). This marginal facies is dominantly composed of ash organized in cross-laminated bedsets. The marginal facies patches were interpreted as resulting from dilute and turbulent currents that were created locally where the main flow bodies would pass a cliff and incorporate large amounts of air (Douillet et al. 2013a.).

These dune bedform fields represent the unique deposits of this type worldwide as they can be investigated both in terms of surficial shape, extent and internal patterns. A downstream decrease in their dimensions (Douillet et al. 2013a) and evolution of outer shape has been recognized (Douillet et al. 2013b). Four types of shapes were defined (Fig 1), and a spatial transition was documented from "elongate" (in proximal zones), "transverse" (at the onset of deposition zones), sinusoidal and "lunate" (intermediate in individual deposition zones), to "2D" bedforms (in the most distal zones of spreading). This organization is very similar to that observed in the behavior of experimental turbidity currents (Spinewine et al. 2009).

2.2. The sediment plate dataset

The dataset consists of ca. 50 m^2 of outcrops from the 2006 deposits. The outcrop sections were hardened in their primary arrangement by impregnating the surface with epoxy, creating sediment plates, a type of thick lacquer peels (method described in Douillet et al., in press.). The difference in resin uptake according to capillary forces (deriving from the grain size distribution) for each lamina pronounces sedimentary structures in the resulting plate, so that stratification is enhanced and underlined to a level of detail that would not otherwise be accessible.

Sets of plates were created for each of the four types of dune bedforms previously recognized in Douillet et al. (2013b): "elongate", "transverse", "lunate" and "2D" (Fig 1). For each bedform, a transect consisted of a 3 m-long outcrop cut perpendicular to the crest, from the superficial stoss-base to the lee, if possible over the entire thickness of the 2006 deposits (1 to 2.2 m).

For the transverse and lunate bedforms, several sets parallel to each other were impregnated, in order to document lateral variations within a single bedform (Fig 2, 3, 4). Further, plates oriented perpendicularly to the inferred flow direction were created to infer lateral continuities (Fig 12, 14). Finally, one 6 m long set was created from the stoss side of the transverse bedform to the crest of the next one, in order to image the connection between successive structures (Fig 3, sets T1a-T1b). One set of plates was made for an "elongate" bedform (Fig 15), a "lunate" bedform in the Chontal area (later on "Chontal" transect, Fig 16), and two sets in two successive "2D" bedforms (Fig 17). A total of 12 sets of 6 plates, each 50 cm wide, were collected and exploitable after transport.

3. Sedimentary structures and facies

The dune bedforms are organized in laminasets and bedsets with coherent patterns separated by sharp unconformities (Fig 3, 4). The general stratal architecture is characterized by partially

preserved lee-side (downstream dipping) bedsets, truncated by long erosive planes. These truncations are either sub-horizontal or very steep (see below) and subsequently covered by sets of backset laminae (upstream dipping). No conventional ripple beds were observed. Single bedforms are compound of several facies types and unconformities. Whereas the transverse and lunate bedforms are largely dominated by well-laminated sets of ash-size clasts (<2 mm), two "2D" bedforms and a second lunate ("Chontal") bedform were found to have an almost massive fabric, consisting of an unsorted mixture of ash (0 to 2 mm diam.), up to blocks (>5.6 cm diam.). The "elongate" bedform investigated here is transitional between these coarse- and fine-grained end members. Hereafter, we describe the main stratification facies based on the observations of the ash dominated bedforms (Transverse, Lunate), and describe the lateral variations between parallel transects in single bedforms (Transverse, Lunate). The coarse grained features (Chontal, 2D1, 2D2) are inventoried and discussed below in section 5 (Fig 15-17).

3.1. Stoss features

a. Steep truncation trains

The most striking and ubiquitous features are steep truncations that cut into the body of the bedforms from upstream (Fig 5). These erosive contacts are subplanar over at least one meter distance in their upstream part. They evolve through a sudden break in angle to steep truncations between 35 and 90º to the horizontal (Fig 5a-b). The downstream termination of these truncations reaches the limit of the paleo-surface where the crest smoothens and vanishes into apparently concordant lee-side laminae. In several cases, the continuation of truncations evolve on the lee side into horizons containing shear structures which formed contemporaneously with the erosive cut (see 3.2 and Douillet et al. sub). Interestingly, these structures repeat in nearby patches (Fig 5a, 7b). Subsequent truncations generally cut through the filling of the former one (stacking upstream from each other). Truncations within a patch have relatively similar dimensions but tend to become steeper in successive occurrences.

b. Steep backsets lineations

The holes that formed in response to the steep truncation events are always subsequently filled with a "steep backset lineation" facies (Fig 5). The material forming the infill can either 1) have a similar grain-size distribution as the undercut laminae (Fig 5a), 2) be richer in coarser clasts, 3) be depleted in fines or 4) be coarser as well as fines-depleted together. The texture of the filling ranges from a massive fabrics with clast-alignment patterns, to "lineated" or laminated. We use lineation here to stress that some coherent sets of outlines are present, but they cannot be confidently interpreted as depositional "laminae", as they may also correspond to secondary truncations within a massive deposit. All of these stratigraphic indicators (truncation line, fabrics, lineations, laminations) render a coherent infill plane that spans angles from 90º to <30º, adopting the morphology of the cutting, and smoothing it over deposition of successive beds.

The basal (upstream) termination of these pseudo-strata are downlaps that approach the base of truncations tangentially, whereas toplaps either organize as converging bundles, evolve into concordant pure-aggradational crests (see 3.2.a), or form splay and fade structures. The resulting sets have roughly the shape of very steep sigmoids. The steep backset lineations evolve progressively away (upstream) from the erosion lines into smoother lenses or become re-incised by a subsequent truncation.

c. Erosive-based backsets

The combination of steep truncations covered with steep backset lineations are always found together, and form what is defined as "erosive-based backsets" (Fig 5a-c, 7b). Those correspond to what is often described or interpreted as so-called "chute-and-pools", a term that implies deposition dominated by a

Froude-jump (a jump in flow Froude-regine, like a hydraulic jump), and thus intrinsically contains a non-proven interpretation (see e.g. Schmincke et al. 1973, Gençalioğlu-Kuşcu et al. 2007, Brand and Clarke 2009).

Interestingly, the erosive-based backsets are visible at multiple scales with invariant morphology, and span over two orders of magnitude with trough-to-crest heights ranging from less than 5 cm (Fig 5c) to >1 m (Fig 5a). In occasions, the structural scale is correlated with the grain size distribution of the subsequent infill (e.g. Fig 5a vs 5c). The smallest examples are, however, exclusively found at the base of the 2006 deposits, in a bedset formed of light grey silt-size ash (Fig 5c, 10). Many small-scale erosive-based backsets are found as lee-side features, with a continuous transition to the backset ripple facies visible on lee sides (see 3.3., Fig 7a).

d. Overturning truncations

The preserved laminasets immediately below truncation planes are occasionally recumbent and overturned in the downflow direction on a thickness of about 1 cm and over lengths up to 15 cm (Fig 5d). These features could be reproduced by analogue experiments using air jets creating short lived bursts and are beyond the scope of this paper (see Douillet et al. 2017). Briefly, they are interpreted as the signature of strong basal bursts or swirls that impact the stoss-face of bedforms. This locally produces an erosive airflow that is so strong that it infiltrates within the bed and coherently disturbs and overturns the particle bed.

e. Planar truncations

Planar truncations are common and seem to be parallel to the local slope over a decameter scale. They occur either as the upstream continuity of the steep truncation events, or reach a paleo-surface where they vanish as apparently concordant beds. Occasionally, some planar truncations cut through the whole length of a bedform (Transverse plate T1a, Elongate, 2D1, 2D2, and Chontal). They are, however, not to be interpreted as a global feature linked with one particular flow event at the eruption scale (Fig 6a).

3.2. Crest features

a. Pure aggradation crests

In several occurrences, the knick point of paleo-crests at a given stratigraphic level exhibits continuous lamination that is preserved from the stoss to the lee side (net deposition on both sides, Fig 6a, 6b). Further, the crest point is found to be shifted laterally between successive laminae, and in most cases, in the upstream direction (as described for the "regressive climbing dunes" in Douillet et al. 2013b). This shift of the crestlines does, however, not represent a migration of the whole structures, (since the root and body of the bedforms are not translated themselves) but results from preferential deposition on stoss faces.

b. Prograding laminasets in regressive bedsets

On the stoss-side of bedforms, individual beds seemingly massive and stoss-aggrading are in fact compounds of thin, oblique, prograding laminasets of higher order –i.e. of finer scale- (Fig 6c). The geometry of the containing beds is clearly stoss-aggrading (which has often been interpreted as indicating Froude-supercritical flow conditions), and an upstream shift of the crest is visible. However, the individual laminae inside a bed are prograding i.e. with accretion in the downstream direction. Upon passing the crest of the bedform, those beds vanish on the lee side.

3.3. Lee side features

a Planar lee laminasets

Lee sides are largely dominated by steeply dipping, planar laminasets (from 10 to >25º). These show strong variations in terms of lamination intensity, ranging from massive thin layers, to diffuse sub-planar beds, and up to very crude and well developed laminasets. These variable planar facies mainly consist of ash and the fabrics range from well-sorted to unsorted at the lamina scale, involving any types of doublets from coarse to medium ash, sometimes also including lapilli horizons or anecdotic outsized clasts (up to 10 cm diam., see paragraph 3.4, Fig 9). When preserved, a continuation with stoss-aggrading beds of any kind is observed. Planar lee-side laminasets are often truncated, and testify that only a small part of the sedimentary history on stoss faces is preserved.

b**. Backset ripples**

Numerous ripple-sized structures (albeit not necessarily genetically, but with similar dimensions, ca. 10 to 30 cm length) with clear stoss aggradation and preferential upstream deposition are found as part of the lee of bedforms, intercalated within the planar laminasets (Fig 7). They seem to be stacked on each other (in duplex), or occur with 2 or 3 periodic repetitions within a synchronous bed (Fig 7a). Such backset ripples occur in close vicinity from the smaller erosive-based backsets, sometimes even in train on the same horizon/isochronous surface (Fig 7a). In few occurrences, these backset ripples can locally evolve into a preferential downstream aggradation trend when aggrading in the stratigraphy, before returning to a regressive trend (Fig 7b). Some of the backset ripples tend to be longer and flattened (ca. 30 cm long and 5 cm thick) as well as amalgamating together, resembling small-scale hummocky-cross-stratification.

c**. Overturned shark fin structures**

Many horizons seem to be at the limit between erosive and concordant and occur superimposed on the planar lamination trend. They include peculiar soft sediment deformation features which are overturned in the flow direction and with a shark fin shape (ca. 1 cm thick; 4 cm long, Fig 8). Such "shark fins" are found to be preceded upstream by a "ploughed zone" suggesting a downstream migration. They were thus interpreted as shear horizons related to traction carpets on lee sides (Douillet et al. 2015). More than 200 shark fins were analyzed and are the focus of the companion manuscript (Douillet et al. sub). The shark fins further occur in periodic trains on an isochrone surface, and a wave mechanism was inferred to explain their formation. A linear stability analysis showed that waves can develop at a shear interface without being linked with surface tension or a density driven restoring force (Douillet et al. sub). Shark fins often occur downstream erosive paleo crests, where the erosive line vanishes into concordant beds.

3.4. Coarse-rich trough fillings

The troughs lying between the base of a lee and stoss of the following bedform often exhibit horizons containing lags of coarser material (Fig 9). Three main types of basal coarse lenses were observed:

a. Superficial lags (Fig 9a): the whole surface of the 2006 bedform fields was covered by a pluri-centimetric layer of centimeter diameter, low density pyroclasts landed by fallout. A lens of similar clasts is systematically accumulated at the base of the stoss faces. Its thickness varies around 3-10 cm.

b. Outsized-clasts horizons (Fig 9b): A horizon in otherwise ash dominated bedsets contains several largely outsized clasts up to >20 cm diameter. Such sporadic and anomalous horizons

are laterally fining into diffuse beds of centimeter-diameter clasts on their upstream continuation, and vanish completely farther downstream.

c. Massive lenses and lensoidal layers (Fig 9c): a massive and relatively coarse-rich (including clasts up to 5 cm) layer thickens to >10 cm on the stoss of a paleo bedform. It can be followed over to the crest, but vanishes within 10s cm downstream on the lee side. In the elongate bedform, the basal part of such a layer also exhibits a short dike and soft sediment deformation that was interpreted as a brief intraflow injected during flow (Douillet et al. sub).

4. Architecture

4.1. Basal contact

The base of the 2006 deposits is visible in the transverse and lunate sediment plates (Fig 10). When exposed, the basal unit is a thick cross-laminated bed (ca. 10 cm) of fine ash overlying coarse and weathered blocks. This zone contains numerous plant remnants, few of them carbonized, and the lamination exhibits a variety of bedding patterns. Small (few cm thick) backset ripples and erosive backsets are present. During digging out the outcrops, non-carbonized plastic ropes and farming remnants were excavated. The basal unit grades abruptly (within a few centimeters) into massive to well laminated, unsorted fine to coarse-grained ash. This latter content forms the majority of the 2006 deposits up to the surface for the transverse and lunate outcrops.

4.2. Lateral variations

Correlations between transects are not apparent, even when separated by <1 m within a single bedform. Overall, a dune bedform outcrop can in no case be taken as a 2D structure, and interpretations may vary drastically within tens of centimeters. An example is suggested on the transverse (Fig 11-12) and lunate (Fig 13-14) bedforms based on the main truncations features and subsequent sedimentary facies as well as cross-profiles.

a. Transverse

The transverse set consists of four flow-parallel transects (T1-T4, Fig 11) and one perpendicular cross-profile (CP, Fig 12) linking the T3 and T4 plates in the crest area. The base of the 2006 eruption is visible in all transects but for T2.

Transect T1 is 6 m long (T1a & T1b). It has its upstream limit aligned with the 3 parallel transects but it extends farther down to the downstream following dune crest. T1a is largely compound of downstream dipping beds lying over the basal contact of the 2006 deposits. These beds are, however, the theater for numerous trains of backset ripples and erosive-based backsets. Some shark fin structures are found on relatively isochrone beds on the lee side. The lower part of T1b presents the character of an aggrading low angle bedform, which is subsequently truncated, with the final structure developing downstream from the paleo-bedform. An outsized clast horizon is present in the trough between both bedforms in the lower third infill part of the 2006 deposits. The stoss side of both successive crests consists of a large scale erosive backset zone terminating as unconformable topsets at the surface. Both of these stoss erosive backsets are not synchronous, and the genesis of the downstream bedform (T1b) pre-dated the final shaping of the upstream one (T1a). A long planar truncation that cuts through the upper part of the whole T1a bedform is lost into conformable beds over the lower lee side.

Transect T2 contrasts in its structural patterns with those of T1. Whereas the base is not exposed, the planar truncation can still be recognized. From T2 on to the following profiles, several series of steep truncations are visible, and may have been confounded as a single

truncation in T1. The four stoss-truncations identified in T2 are steepening the bedform, and are followed by episodes of stoss deposition and crest aggradation.

Transect T3 marks the onset of subvertical truncation trains. It is the steepest part of the bedform, and up to 7 trains of steep subvertical truncations followed by stoss aggrading beds are preserved. They can be correlated to some of the T2 truncations events through their stratigraphic position, the degree of truncation, and the nature of the infill that contains faint lineations, some centimetric outsized clasts including light grey pumice lapilli clasts.

Transect T4 is located below the crest edge of the bedform. Five distinct packages of truncation trains are exposed. The main train of backset laminae is translating in the upstream direction over more than 1.5 m.

A cross-profile connecting T3 and T4 was made in the crest area (Fig 12). It exhibits as much variability as the flow-parallel profiles. Truncation events are sometimes recognized, and seen to evolve with steep angles in the flow-perpendicular direction. They also cross cut each other, which explains the complications upon the correlation of the individual profiles.

b. Lunate

The three lunate transects show more similarities between each other and the correlations are more confidently proposed (Fig 13, 14). This bedform is located just 10 m upstream from the transverse one, so that the same color-code is used, that may relate to the same flow events as for the transverse bedform.

The first major truncation event visible in transects T2 and TN lies ca. 25 to 50 cm above the basal fine-grained unit. This truncation surface is planar to downstream dipping, and overlain by a coarse-rich horizon, a combination similar to the transect T1 and T2 from the transverse bedform. Two additional truncative surfaces occur 20 to 40 cm higher in the stratigraphy, and are planar downstream to slightly upstream dipping. The stoss side of the lunate bedform is, as for the transverse one, cut by, three steep truncation planes that can be correlated through the different profiles. The trough upstream from the stoss face is finally partially filled with a lens of light pyroclasts similar to the final fallout covering the surface. A distinct discordance on the upper part of the lee of transects T2 and TN-1 has been interpreted as a very short-throw slumping event that produced a horizon with convolute and disturbed soft sediment deformation features (Douillet et a. sub).

Three successive cross-profile plates were created between TN-1 and TN and confirm the correlations of truncation surfaces between transects (Fig 14). Interestingly, the same richness of structures and amount of variability is visible in the cross-profiles thought to be perpendicular to the flow direction. In particular, numerous shark fin structures, backset ripples, and small erosive-based backset beds are visible. Whether these small-scale structures are related to varying flow direction or to local slope-related transport processes on the outer tail of the lunate bedform is unclear.

5. Coarse-grained bedforms

5.1. Elongate

The elongate transect is transitional between the fine-grained bedforms and the coarser-grained ones (Fig 15). It contains ash to lapilli clasts, organized in diffusely laminated bedsets to massive layers up to 15 cm thick. Overall the bedform has a low angle structure and little in common with the other ones in terms of stratal architecture. The base of the 2006 deposits could not be observed in nearby rain-gullies cutting several meters down the surface. Sub-planar, downstream dipping laminasets of low angle cross-laminations cut into each other in the lower part. A low angle proto-bedform developed in the middle part of the plate, and consists of diffuse

and low angle backset beds. This structure is then covered by several massive to faintly stratified layers with a grading contact. The latter layers are stacking up on the stoss of each other, resulting in a regressive lensoidal structure.

5.2. Chontal

The Chontal bedform has the outer shape of a relatively flat lunate bedform, yet its internal content is completely distinct from lunate bedform described earlier (Fig 16). It lies on the shoulder of two valleys that directed pyroclastic currents and come closer together before a sharp curve, so that the influence of two pyroclastic currents with diverging flow directions was hypothesized (see the "Chontal" area in Douillet et al. 2013a). The base of the 2006 deposits could not be reached, although a height of > 2 m was exposed.

Three main sedimentary phases can be identified:

-In the lower part, a unit of ash-dominated bedsets (>50 cm thick) containing small erosive-based backsets and planar truncations is exposed. Its content is relatively coarse, with centimetric clasts that are concentrated in the backsets' trough. This lower part contrasts with the rest of the bedform, and its upper contact is sharp, although without clear sign of any truncation. This unit might be related to the July 2006 pyroclastic currents rather than the ones from August.

-A very coarse and unsorted unit (ca. 1.7 m thick) containing clasts from the ash size to blocks up to ca. 10 cm diameter covers the lower ash bedsets. Whereas it appears as fairly massive at the outcrop, the corresponding sediment plate exhibits several structures highlighted through an undefined but perceived lineation trend. On the stoss side, signs of large and very steep (70-90º) backset lineations are visible on the upper part, forming diffuse splay and fade structures. They evolve into less steep backset lines over a thickness of ca. 1 m. On the lee side, planar lineations are perceived. They are superimposed with a clear fining up gradient. This sedimentary facies is referred to as "coarse-lineated" in the following (chapter 6.4.).

-Finally, the third unit (10 to 35 cm thick) consists of a bedset that becomes diffusely laminated, with a greater thickness on the stoss than on the lee side. Ash laminations are intercalated with more massive and fining up layers.

5.3. 2D bedforms

The two 2D bedforms are located in an area on the counter-slope of the volcano flanks, past the base of the edifice. The parental flows must have crossed the valley of the Chambo river, and were interpreted as spreading against the local slope at the downstream limit of inundation of the pyroclastic currents. The base of the deposits was not encountered with the sediment plates, yet erosive rain-gullies testify a local thickness >4 meters.

The lower part of the transect is massive, unsorted, including blocks up to 15 cm diameter (Fig 17). It is overlain by a diffusely laminated, finer grained bedset, ca. 30 cm thick.

Both units are truncated on their stoss face by a layer with evidence for (i) the occurrence of deposition on the stoss-side, (i) backset lineations visible in the "2D1" bedform, and (iii) a locally very varying nature from massive to diffuse lamination. Finally, a low angle, second truncation of the stoss face is covered by another bedset of diffuse to massive layers consisting of ash to lapilli clasts.

6. Interpretation

The numerous sedimentary features exposed in the dataset bring a range of questions. There are two ways to interpret their formation. In the "traditional" scheme, the flow regime would dictate the sedimentation processes. Here, the occurrence of stoss-side deposition would thus be

interpreted as indicating Froude-supercritical or transcritical antidunes and chute and pools. In this frame, relatively stable flows and the oscillation of a free upper surface would be needed. However, we do not favor this interpretation since experimental and observational evidences about pyroclastic currents point toward pulsating and unsteady flows (e.g. Hoblitt 1986, Brown et al. 2007, Andrews and Manga 2012, Breard and Lube, 2016) where no stable conditions could develop. In this context, we open a discussion and revision of the generally accepted distinctive features to interpret sedimentary structures related to Froude-supercritical flows. We show that the bedforms' structural patterns can be well explained by mechanisms driven by the basal topography and bed shapes that would interact with flow bursts and pulses in highly turbulent flows at very high sedimentation rates.

6.1. Steepness and lateral variations: the invalidation of flow regime interpretations

The transverse bedform drastically evolves in terms of stratal architecture over the four lateral profiles (Fig 3, 11-12). If put in a flow-regime interpretation, T1 would likely be interpreted as a subcritical dune, T2 as an antidune, whereas T3 and T4 would represent chute and pool structures. It has been suggested that antidunes (indicating Froude-supercritical flows) would occur in more proximal areas than chute and pools (indicating hydraulic jumps / Froude jumps), and that distal deposits would in turn be dominated by subcritical bedforms (e.g. Schmincke et al. 1973). Our data invalidates this model, since the three types of stratal architectures coexist in the same structure and on the same horizon. We consider it very unlikely that three distinct flow regimes are recorded within few meters of one another, within a single bedform, and at the same time. Indeed, we cannot explain how a flow could be radically distorted in Froude-regime so that a single structure would coexist within three different parts of a bedforms' phase diagram.

Additionally, the extreme steepness of the backset beds contrasts with the experimental evidences of bedding related to Froude-supercritical flows, which are generally at low angle and cross-cutting each other (e.g. Alexander et al 2001, Cartigny et al. 2014, Vellinga et al. 2018). As already pointed from their surface expression, the geometrical relationships of the bedforms' dimensions and their steepness are not compatible with Froude-supercritical flows (Douillet et al. 2013b), an argument further exacerbated by the internal patterns evidenced here. Finally, lee side erosion is virtually absent from the outcrops, an observation that excludes their interpretation as antidunes. Indeed, antidunes form as a mould of a gravity wave and contain backset bedding when the wave migrates upstream, a feature that should thus be associated with concurrent lee-side erosion due to this same upstream migration of the wave.

In this context, we show that all sedimentary features evidenced here can be interpreted without involving a flow in Froude-supercritical regime (see next chapters). We suggest that the sedimentary architecture of the structures is dominated by the flow unsteadiness and turbulence (related to the Reynolds dimensionless number) rather than by the flow regime (defined through the Froude dimensionless number). In particular backset bedding is related to highly depositional and slow currents with depletive and waning dynamics.

6.2. Turbulent bursts

a. Scale invariant features and turbulent vortices

The erosive-based backset structures show a striking scale-invariance of the patterns over 2 orders of magnitude (Fig 5, 10). The largest documented examples in the literature (at Laacher See, Germany) reach a scale of several meters and are formed by very coarse-grained lapilli (pebble-size) pumice clasts with a similar stratal architecture (see Figure 8 in Douillet et al. in press, Schmincke et al. 1973). If a dimensional scaling could be simply translated between the

size of the structures to their parental flow process, then this would mean that the same flow processes occur at different scales. A scale-invariant flow process that could form steep truncations can be related to turbulent eddies. Indeed, the eddy downscale-cascading inherent to turbulent flows (see Kolmogorov scale /enstrophy cascade rate, e.g. Vallis 2006, pp.341-349) predicts such eddies from the flow scale to the centimeter scale.

Recent large-scale pyroclastic current experiments further showed that mesoscale turbulence clusters would form and concentrate particles outside turbulent eddies (Breard et al. 2016). We suggest that such turbulent clusters inherent to pyroclastic currents could impact on the stoss face of bedforms as erosive bursts, followed by highly depositional moments and form erosive-based backsets. This possibility is to be verified through Reynolds-scaled analogue or numerical modeling as well as further field investigations on the genetic and timing relations between successive truncations.

b. Narrow timescales and high sedimentation

The sub-vertical truncations and subsequent sub-vertical backset beds as fillings suggest highly and fast varying phenomenon (Fig 5a). Their occurrence as subsequent repetitive trains in a single nest further suggests a pulsating behavior of flushing away and deposition within a narrow time window. In the absence of cohesive forces, the organization of the filling as subvertical aggrading lamination inside a truncation nest could unlikely be preserved without extremely fast burial to avoid gravitational collapse. Thus, very high sedimentation rates with deposition of laminasets several tens of centimeters thick must have occurred within seconds within a pressing/plastering current. Such sharp transitions in sedimentary behavior testify the highly turbulent nature of the flows with sudden evolution between extremes of erosive and depositional behaviors.

Experimental turbidity currents also exhibit a pulsating behavior with short time recurrences (Cartigny et al. 2013), whereas experimental turbulent pyroclastic currents form "series of sedimentation–erosion couplets that propagate" across the flow bed interface (Andrews and Manga 2012). Such erosion-sedimentation couplets would well explain the subsequent backset re-incisions. Considering the formation of sedimentary steep backsets and backset ripples, our interpretation is that their growth is the sole consequence of high sedimentation rates against basal topographic obstacles, and their position dictated by the local topography. Indeed, if sedimentation is high enough that any bed irregularity would trigger the formation of backset beds as a flow reaction, a self-sustaining process can occur, as seem to be visible. Further, scale would not be involved in such a process and this would explain why the same patterns are obtained at several sizes.

c. Coherent turbulent structures

In 3D, the lateral variations are found to be abruptly evolving, with continuity of the order of less than a meter and crest-perpendicular truncation angles up to >30º (Fig 12). This emphasizes that the transient phenomenon cutting bedforms are also very localized. In addition, the truncations that likely remobilized large amounts of pre-deposited material are also evolving within tens of centimeters in the downstream direction into concordant aggrading planes. This indicates locally waning conditions, and that processes of recycling and cannibalism of the sedimentary structures over short distances dominate the dynamics.

Most erosional furrows and sharp scouring of bedforms in the literature, regarded independently of a specific environment, have been perceived as resulting from coherent turbulent cells (e.g. Richards 1959, Fisher 1977, Kieffer and Sturtevan 1988, Dumas et al. 2005). Numerical simulations of turbulent structures over ripple beds have shown that coherent

structures identified as "Görtler vortices" could form and be a main agent of sediment entrainment (e.g. Zedler et al. 2001). If occurring at the meter scale in pyroclastic currents, such Görtler vortices would be very appropriate flow-structures to explain the formation of steep truncation events. In subaqueous experiments, the scouring of stoss-faces described by Dumas et al (2005) could be attributed to a similar effect. At high Reynold numbers, numerical simulations succeed in reproducing low- and high-speed streaks that could impact the stoss faces of bedforms (e.g. Cantero et al. 2008). We speculate that such streaks or Görtler vortices could be the dominant mechanism that shape the stratal architecture of erosive backset events, in a similar manner as for smaller scale bedforms and the scouring described by Dumas et al (2005). Alternatively, pulsating Froude-jumps might produce similar features, yet natural observations of these processes are almost exclusively linked with lee side erosion (e.g. Dietrich et al. 2016, Hage et al. 2018) and no argument allows to solve this question.

The steep truncations and backset lineations are similar to what is generally interpreted as chute and pools (e.g. types I, II, IX of Schmincke et al. 1973, types d and e of Cole 1991), and our revised interpretation may be applicable for all those structures.

6.3. Coarse bedforms: the transitional limit between granular and turbulent flows

a. Coarse lineated facies: locally turbulent flows

The imaging power of the impregnation method enabled the identification of subtle lineation/lamination patterns even in the coarsest and most unsorted bedforms (e.g. Chontal & 2D outcrops). The parental currents were likely dominated by particle-particle interactions during their transportational phase in order to support the coarse content of the deposits, an hypothesis reinforced by the bad sorting of this facies (Fig 16, 17). However, the faint occurrence of backset and aggrading crest lineations point toward tractional transport, likely related to mechanisms of support locally driven by the fluid's turbulence. These bedforms may thus represent deposits recording the hypothesized transitional flow behavior between "concentrated" (granular) and "dilute" (turbulent) end members of pyroclastic currents (e.g. Burgisser and Bergantz 2002). This strengthens our previous interpretation that the flows responsible for the marginal overbank deposits locally emanate from valley-confined granular flows when a portion of these became turbulent as a result of air entrainment upon passing upstream cliffs (Douillet et al. 2013a). The closest processes that might explain this coarse-lineated sedimentary facies are found in the dam break analogue experiments conducted by Rowley et al (2014), where fluidized flows deposited backset, lineated beds. Leclair and Arnott (2005) showed that turbidity currents with up to 36% particle concentration in the bedload layer could deposit as laminated beds, and this ratio is suggested as an order of concentration here. The fining-up, grading trends may represent a local decrease in flow competence or energy but any link to the eruption dynamics is refrained.

The existence of the coarse-lineated facies further reconciles the observation that zones where the 2006 currents were interpreted as weak occurred concurrently with broken tree logs, 10s cm in diameter. The tilting and breaking of the logs can be imputed to the locally turbulent coarse flows (responsible for the coarse lineated facies) rather than the turbulent currents dominated by ash and weak deposition.

b. Coarse lags: topographic pools

The superficial lags at the base of stoss faces, formed by clasts similar to the final fallout event that drape the 2006 deposits seem straightforward to interpret as a result of slight reworking and winnowing of the finer-grained material by rain or wind (Fig 9a). Such features, clearly

interpretable here, could however be very misleading in paleo-studies where several flows are stacked on top of each other.

Outsized clast horizons within the 2006 succession and with their isochronous, upstream and downstream fading into ash dominated lamination emphasize that the grain size of the deposits is not a simple function of travel distance or flow energy, but strongly influenced by local topographic obstacles (Fig 9b). These horizons may represent some anecdotic pulses of granular flows or increased bedload transport. Whereas the flow capacity must be exceeded over the whole lateral continuation of the bed in order for sedimentation to occur, the competence seems to have been large enough to transport large clasts down to the troughs, but insufficient to transport them out of the troughs (see e.g. Hiscott 1994).

Following our previous interpretation (Douillet et al. 2013b, Douillet et al, sub) the massive, unsorted and coarse-grained nature of the lenses and lensoidal layers are considered to result from parent flows with dominant particle-particle support (granular flows or bedload rich) over a thickness at least equalling the size of the largest transported clasts rather than fluid turbulence support down to the flow-bed boundary (Fig 9c). The lenses vanish outside the troughs formed by the upstream toe of stoss-faces and so, they flatten topography by filling the troughs. They can be understood as the signature of a simple damming triggered in the pools at the toe of bedforms. No particular flow conditions are required and this is understood as a pure topography-triggered jamming or frictional freezing, due to the parental "granular" part of the flows tripping against the obstacle formed by bedforms (see also the caterpillar effect and intrabed flows in Douillet et al. sub).

6.4. Four-fold formation mechanisms

All together, the outcrops from Tungurahua enable construction of a depositional scheme for pyroclastic bedforms compound of four formational bricks (Fig 18).

a. Differential draping fallout

The purely aggrading crests resemble climbing structures (ripples or dunes), apart for their upstream preferential deposition (Fig 6a, 6b, 7). Climbing structures are generally interpreted as resulting from sedimentation with higher depositional rates than translational (e.g. Allen 1971, Ashley et al. 1982). In proglacial settings, climbing-dune-cross-stratifications are related to high rates of transfer of sands from suspension to the bed and net deposition on a bedform's stoss-sides (Ghienne et al. 2010), a result likely transferable here. As already suggested for turbidites (Ponce and Carmona 2011) and pyroclastic currents (Douillet et al. 2013b), we interpret that the stoss-depositional crests result from a process of differential draping, whereby fallout-dominated deposition is enhanced on stoss-faces, due to the simple combination of the bed topography and trajectory of particles (Fig 18b). This requires the bedsets to be sedimented in a gentle current with shear velocities below the saltation threshold, and high fallout input. The fallout load would originate from upper parts of the pyroclastic currents, because of spatial and/or temporal changes in sediment transport rate.

The median diameter (Md) previously measured for the Tungurahua 2006 pyroclastic bedforms is around Md=2 Phi (Douillet et al. 2013a) and can be used with the corresponding shear velocity (u*) at the saltation threshold measured for a flat bed in a wind tunnel (Douillet et al. 2014). This would imply that purely aggrading crests were emplaced by weak currents with shear velocities below $u^*=0.29$ m.s^{-1}, corresponding to near-bed velocities below 6 m.s^{-1} at a height of 10 cm above the bed for a pure wind.

b. Slope-influenced saltation

The regressive laminasets found on stoss faces, which internally consist of prograding individual laminae, that vanish downstream a crest (Fig 6c) are understood here as representing slightly higher shear velocities than for differential draping bedsets. For these beds, the saltation threshold is partially reached, so that particles are transported near the bed and produce prograding laminae. Whereas the saltation transport is sufficient to transport away all particles downslope and thus no deposition occurs on a lee side, it has a net loss of carriage on stoss faces (Fig 18c). This is supported by wind tunnel measurements of the saltation threshold for pyroclasts at various bedslopes, where it was measured that the threshold is reached at up to 50% more shear velocity on a +25º slope than on a downstream dipping bed with a -25º slope (Douillet et al. 2014). Following the same comparison to wind tunnel measurements as before for the prograding stoss-laminasets, the shear velocities needed considering that the saltation threshold is reached on stoss-faces ($u^* \sim 0.39$ m.s^{-1}) and surpassed on lee faces ($u^* > 0.27$ m.s^{-1}) means that velocities of ca. 8 m.s^{-1} (for a pure wind) would be needed at 10 cm above the bed, slightly above the one for pure aggrading crests.

c. Truncative bursts

The steep truncations represent anomalies that disturb the previous weak-current sedimentary processes (Fig 5). Short lived, highly erosive basal pulses related to coherent turbulent structures at the flow-bed boundary are the best candidate to explain these features, and they represent the high-energy moments of the pyroclastic currents (Fig 18d). These are directly followed by moments of very high deposition, yet lateral velocities must be present to ensure that subvertical lamination is plastered against those truncations. Those turbulent high velocity clusters must be advected in the downstream direction as well as close to the bed, in order to mainly impact on stoss faces, yet smaller ones seem to brush lee faces as well. In order to produce overturning at truncations as observed in the deposits, burst jets with velocities ranging from 28-40 m.s^{-1} were needed in small scale experiments (Douillet et al. 2017), which is taken as a lower range value for the real deposits of Tungurahua, largely above the values for aggrading phases.

d. Granular-based events

The coarse and massive lensoidal layers that punctually agreement bedforms' patterns represent the granular-flow part of the bedform-forming pyroclastic currents (Fig 9b-c, 18e). These sporadic events may be more common than their sedimentary signature, since the lenses often vanish as sedimentary bypasses, with no information on a granular-based passage. The flows were probably at least as thick as the coarsest deposited clasts (see 6.3.b). Interestingly, experimental granular flows passing over a bedform experience a jump similar to a Froude-jump (granular jump) and could leave a similar sedimentary signature (Viroulet et al. 2017).

e. Four mechanisms and no equilibrium conditions

The whole variety of Tungurahua's bedforms can be reconstructed with a combination of the four formation mechanisms, and more generally, can be applied to most pyroclastic bedform deposits elsewhere. Notably, such pyroclastic structures do not exhibit any kind of equilibrium bedform (e.g. sustained progradation/translation). This is likely a result of rapidly changing conditions and the absence of any stable flow over intervals comparable to the timescales of growth of a sedimentary structure. These bedforms are a simple stack of the four depositional processes interacting with the pre-deposited structures. This disequilibrium is further supported by the systematic spatial stability of pyroclastic bedforms, at Tungurahua and

elsewhere: Once a bed morphology is initiated, no migration is observed, over several meters thickness of deposition and through the variety of depositional mechanisms. Hence no stable conditions were reached during the flow of the parent pyroclastic current.

6.5. Flow energy

When interpreting sediments, we probably never look at the moments of the flow where it has its highest energy, but only at the ones where deposition occur, likely always during vanishing periods. As such, sediments are thus unlikely to reflect any high energy events. The most erosive, and indirectly, energetic events, reported here, are the truncative bursts. All stoss-aggrading features are interpreted here as low energy events. This is further supported by the fact that the final depositional bedsets almost always contain strong stoss-aggrading patterns. Thus stoss-aggradation belongs to the waning, rather than are highly energetic periods of a pyroclastic current, when the flows vanish.

Even in an interpretation as "Froude-supercritical bedforms", the sedimentary beds should not be related to high energy flows. Indeed, although many interpretations refer to Froude-supercritical flows as highly energetic, this is a confusing statement. The flow regime, defined as sub- or super-critical (or lower and upper flow regime resp.), corresponds to a flow state where the Froude number (Fr) is Fr <1 resp. Fr >1. This ratio informs on the kinetic over potential energy of a flow, but in no way on the amount of total or kinetic energy of the flow. In nature, Froude-supercritical flows may in most cases represent waning, low energy conditions, rather than high energy events. Compared to a subcritical flow, supercritical conditions may well be attained through a decrease in flow depth rather than increase of velocity, and would as such correspond to a decrease in energy. We thus consider that only the truncative events could be related to highly energetic events, if looked at over the temporal sedimentation phases of a flow.

Conclusion

The dataset presented here represents an extensive and fine scale investigation of pyroclastic bedforms and their lateral variations. The sedimentary architecture of the structures largely consists of stoss-aggrading features such as backset ripples, erosive-based backset bedset trains, draping crests with preferential stoss deposition, or lensoidal layers. They are punctuated by important truncation events that attack the stoss-face of bedforms with angles up to the vertical.

The presented structures can be explained through the combination of four formational mechanisms, namely "differential draping", "stoss-influenced saltation", "truncative bursts", and "granular-based pulses". The kinetic energy related to the constructive phases of the sedimentary history is likely very low and involves high rates of sedimentation and weak currents.

Coarse grained, unsorted and apparently massive deposits contain similar truncations and backset beds as laminated bedforms, yet less pronounced. They represent the signature of depositional portion of a current at the transition between turbulent and granular: although granular during transport, the sedimentary dynamics was turbulent enough to produce faint lineations and stratification. They are thus understood as granular currents that have locally become turbulent in the vicinity of their deposition zone and testify the gradual continuum between dense pyroclastic flows (granular-based) and dilute pyroclastic currents (turbulent supported).

The location of a pyroclastic bedform is spatially very stable. This contrasts with the high variability in stratal architecture within a single dune. Within tens of centimeters, truncations

can reach angles of >30º in the flow-perpendicular direction, and pass from sub-vertical truncations to concordant lamination in the flow-parallel direction. All together, the features evidence that no equilibrium is reached, and that these dune bedforms are transient structures. All features point toward very pulsating behavior, and the dominant role of turbulence and local coherent turbulence structures in the vicinity of the bed (possibly Görtler vortices), interacting with the topographic expression of the previously deposited bedform.

Whereas pyroclastic bedforms have long been interpreted as antidunes and chute and pools related to Froude-supercritical flow regime, this interpretation is not favored here. The data shows that the features usually taken as diagnostic for Froude-supercritical bedforms are drastically evolving within a single structure. The interpretation thus puts emphasis on the combined role of pre-existing morphology and local scouring. Accent is put on the high turbulence and extreme sedimentation, hence related to high Reynold numbers within unsteady, weak, and waning currents. Quantitative estimates of nearby flow-velocity are made with comparison to wind tunnel experiments on saltating pyroclasts. They suggest that a pure wind velocity of 6 to 8 $m.s^{-1}$ could emplace the constructive bedsets, whereas the truncative phases would result from bursts at 30-40 $m.s^{-1}$.

Acknowledgements

We are thankful to Ben Andrews and Gert Lube for their fruitful comment**.** This project is supported by the Deutsche Forschungsgemeinschaft grant DO1953/1-1 to GAD. GAD acknowledges financial support by the Bavarian grant Thesis and BayLat. GAD and UK were financially supported by the Deutsche Forschungsgemeinschaft grant KU2689/2-1. QC was supported by the Alsacian grant "Boussole". All field expenses were covered through the support of an ERC Advanced Grant to DBD (247076). GAD, CM, and UK thank the members of the Instituto Geofísico for help at Tungurahua.

Figure captions:

Figure 1: Sketch of the four different bedform shapes identified at Tungurahua. A: Transverse, B: Lunate, C: Elongate, D: 2D.

Figure 2: Surface shape (A resp. B), and the trenches realized to impregnate the transects (C resp. D) for the of the transverse resp. lunate bedform.

Figure 3a and 3b: Transects within the Transverse bedform. Flow toward the center of the book. All transects are formed by 6 individual plates 50 cm broad, forming a 3 m long profile. Transect T1a and T1b connect to form a 6 m long profile.

Figure 4a and 4b: Transects within the lunate bedform. Flow toward the center of the book. All transects are formed by 6 individual plates 50 cm broad, forming a 3 m long profile.

Figure 5: Stoss-side features. A-C: Erosive-based backset trains at different scales, A: Bedform scale (Trans-T4P1-4), B: Vertical truncation with vertical and overhanging infill of backset lineations (Trans-T3P1)., C: Small-scale erosive-based backsets in silt-sized ash. D: Truncation with overturned lamination (Luna-T3P2).

Figure 6: Crest features. A: Pure-aggradation crest bedset building on a stoss-erosive paleo crest and subsequently cut by planar truncation (Trans-T4P4). B: Pure-aggradation crest with upstream preferential deposition in the terminal sedimentation phase of growth (Trans-T2P3-4). C: Regressive (stoss-depositional) beds containing prograding laminasets. Note that laminaset vanish as soon as the paleo-crest is reached (Plate from a previously investigated transverse bedform presented in Douillet et al. 2015).

Figure 7: Backset ripples. A: Patches of backset ripples and erosive-based backset trains (Trans-T4P1). B: Propagation of a backset ripple structure through the stratigraphy, with evolving behavior from preferential stoss- or lee-deposition (regressive and progressive, TransT3P4). The pink line follows the successive position of the crest.

Figure 8: Train of three shark fin structures interpreted as representing shear instabilities at the base of the flow (see Douillet et al. sub).

Figure 9: Coarse-grained lags and lenses. A: Superficial lag formed of light gray pumice (Trans-T1bP3-6). B: Horizon with oversized clasts that vanish laterally into finer grained particles and eventually disappears (Trans-T1bP1-4). C: Relatively coarse and massive lens that forms on the stoss side of a paleo-crest and vanishes on the lee (Trans-T3P3-5).

Figure 10: Basal contact of the 2006 eruption (Trans-T1bP4). Note the coarse and weathered ground overlain by silt-sized ash beds containing uncarbonized orchid leafs (E*pidendrum Jamiesonis*) and fine scale erosive-based backset structures. The sequence is sharply coarsening-up.

Figure 11: A possible correlation of the Transverse transects. Truncations are highlighted with colors that relate to the same bursts on the different transects.

Figure 12: Cross profile (CP) between Trans T3 and Trans T4. A) Plate organization in the field. B) Interpreted relations in the downstream direction.C) Interpreted relations in the upstream direction.

Figure 13: A possible correlation of the Lunate transects. The color coding is based on the same events as for the transverse bedform (these two structures are separated by ca. 10 m in the field).

Figure 14: Cross profiles (CP) between Lunate TN-1 and Lunate TN. A) CP1: upstream toe of bedform B) CP2: above the crest, C) CP3: on the lee-side. D) Plate organization in the field.

Figure 15: Interpreted transect of the Elongate bedform. This bedform is the most proximal, situated ca. 2 km up-valley from the transverse and lunate outcrops. For details on the massive lens and deformed beds, see Douillet et al. sub.

Figure 16: A) Interpreted transect of the bedform from the Chontal area. B) Zoom of the zone highlighted in A reveals the coarse-lineated facies and contact with lowermost unit.

Figure 17: Interpreted transects from the 2D bedforms. These are located in the most distal deposits, situated ca. 500 m down-valley from the transverse and lunate bedforms.

Figure 18: Interpretative sketch of the four formational mechanisms for pyroclastic bedforms. A) General sketch of a bedform, B) Differential draping, C) Stoss-influenced saltation D) Erosive basal bursts, E) Granular jamming.

Tables:

Plate Name	Location (valley)	Latitude	Longitude	Profiles	Type*	GPR**
Lunate	Achupashal	1°25'59.64"S	78°29'28.82"W	3*6	ash strat	No
Transverse	Achupashal	1°25'59.19"S	78°29'28.99"W	3*6+1*12	ash strat and block isol	Yes
Elongate	Achupashal	1°26'36.96"S	78°28'22.08"W	1*6	ash and lapilli strat.	Yes
2D-1	Achupashal	1°26'03.84"S	78°29'48.84"W	1*6	ash strat and lapilli mas	Yes
2D-2	Achupashal	1°26'03.48"S	78°29'48.48"W	1*4	ash strat and lapilli mas	Yes
Chontal	Juive Grande	1°25'49.08"S	78°27'14.40"W	1*6	lapilli mas and strat	Yes

Table 1: Summary of all bedforms investigated
*strat=stratified, mas=massive, isol=isolated
**GPR: A ground penetrating radar (GPR) survey was carried on the bedforms prior to their dissection and is the focus of a forthcoming manuscript - see Dujardin (2014) for preliminary results.

References

Alexander, J., Bridge, J. S., Cheel, R. J., & Leclair, S. F. (2001) Bedforms and associated sedimentary structures formed under supercritical water flows over aggrading sand beds. Sedimentology, 48(1), 133-152

Allen, J.R.L., (1971), A theoretical and experimental study of climbing-ripple cross- lamination, with a field application to the Uppsala Esker: Geografiska Annaler, Series A, Physical Geography, v. 53, p. 157–187.

Andrews, B. J. (2014). Dispersal and air entrainment in unconfined dilute pyroclastic density currents. Bulletin of Volcanology, 76(9), 852.

Andrews, B. J., & Manga, M. (2012). Experimental study of turbulence, sedimentation, and coignimbrite mass partitioning in dilute pyroclastic density currents. Journal of Volcanology and Geothermal Research, 225, 30-44.

Ashley, G.M., Southard, J.B., Boothroyd, J.C., (1982), Deposition of climbing- ripple beds: a flume simulation: Sedimentology, v. 29, p. 67–79.

Balachandar, R., & Reddy, H. P. (2013). Scour caused by wall jets. In Sediment Transport Processes and Their Modelling Applications.(edited by A.J. Manning) InTech.

Brand, B. D., & Clarke, A. B. (2009). The architecture, eruptive history, and evolution of the Table Rock Complex, Oregon: From a Surtseyan to an energetic maar eruption. Journal of Volcanology and Geothermal Research, 180(2-4), 203-224.

Brand, B. D., & Clarke, A. B. (2012). An unusually energetic basaltic phreatomagmatic eruption: using deposit characteristics to constrain dilute pyroclastic density current dynamics. Journal of Volcanology and Geothermal Research, 243, 81-90.

Brand, B. D., & White, C. M. (2007). Origin and stratigraphy of phreatomagmatic deposits at the Pleistocene Sinker Butte volcano, western Snake River Plain, Idaho. Journal of Volcanology and Geothermal Research, 160(3-4), 319-339.

Brand, B. D., Clarke, A. B., & Semken, S. (2009). Eruptive conditions and depositional processes of Narbona Pass Maar volcano, Navajo volcanic field, Navajo Nation, New Mexico (USA). Bulletin of Volcanology, 71(1), 49.

Branney M,.J.,and Kokelaar B.P. 1992. A reappraisal of ignimbrite emplacement: Changes from particulate to non-particulate flow during progressive aggradation of high-grade•Ignimbrite Bull. Volcanol.,54,504-520

Branney, M. J., Kokelaar, P., & Kokelaar, B. P. (2002). Pyroclastic density currents and the sedimentation of ignimbrites. Geological Society of London.

Breard, E. C. P., Lube, G., Cronin, S. J., & Valentine, G. A. (2015). Transport and deposition processes of the hydrothermal blast of the 6 August 2012 Te Maari eruption, Mt. Tongariro. Bulletin of Volcanology, 77(11), 100.

Breard, E. C., Lube, G., Jones, J. R., Dufek, J., Cronin, S. J., Valentine, G. A., & Moebis, A. (2016). Coupling of turbulent and non-turbulent flow regimes within pyroclastic density currents. Nature Geoscience, 9(10), 767.

Brown, R. J., & Branney, M. J. (2004). Bypassing and diachronous deposition from density currents: Evidence from a giant regressive bed form in the Poris ignimbrite, Tenerife, Canary Islands. Geology, 32(5), 445-448.

Brown, R. J., Kokelaar, B. P., & Branney, M. J. (2007). Widespread transport of pyroclastic density currents from a large silicic tuff ring: the Glaramara tuff, Scafell caldera, English Lake District, UK. Sedimentology, 54(5), 1163-1190.

Burgisser A, Bergantz GW (2002) Reconciling pyroclastic flow and surge: The multiphase physics of pyroclastic density currents. Earth Planet Sci Lett 202: 405-418

Bursik MI, Woods AW (2000) The effects of topography on sedimentation from particle-laden turbulent density currents. J Sed Res 70 : 53 - 63

Cantero, M. I., Balachandar, S., García, M. H., & Bock, D. (2008). Turbulent structures in planar gravity currents and their influence on the flow dynamics. Journal of Geophysical Research: Oceans, 113(C8).

Cartigny, M. J. B., Postma, G., van den Berg, J. H. and Mastbergen, D. R. (2011) A comparative study of sediment waves and cyclic steps based on geometries, internal structures and numerical modeling. Mar. Geol., 280, 40–56.

Cartigny, M. J., Eggenhuisen, J. T., Hansen, E. W., & Postma, G. (2013). Concentration-dependent flow stratification in experimental high-density turbidity currents and their relevance to turbidite facies models. Journal of Sedimentary Research, 83(12), 1047-1065.

Cartigny, M. J. B., Ventra, D., Postma, G. and van Den Berg, J. H. (2014) Morphodynamics and sedimentary structures of bedforms under supercritical-flow conditions: new insights from flume experiments. Sedimentology, 61, 712–748.

Charland, A., & Lajoie, J. (1989). Characteristics of pyroclastic deposits at the margin of Fond Canonville, Martinique, and implications for the transport of the 1902 nuées ardentes of Mt. Pelée. Journal of volcanology and geothermal research, 38(1-2), 97-112.

Cole, P. D. (1991). Migration direction of sand-wave structures in pyroclastic-surge deposits: implications for depositional processes. Geology, 19(11), 1108-1111.

Cole P.D., Scarpati C. 1993. A facies interpretation of the eruption and emplacement mechanisms of the upper part of the Neapolitan Yellow Tuff, Campi Flegrei, southern Italy. Bull. Volcanol. 55, 311-326, 1993.

Crowe, B. M., & Fisher, R. V. (1973). Sedimentary structures in base-surge deposits with special reference to cross-bedding, Ubehebe Craters, Death Valley, California. Geological Society of America Bulletin, 84(2), 663-682.

Dellino, P., Isaia, R., & Veneruso, M. (2004a). Turbulent boundary layer shear flows as an approximation of base surges at Campi Flegrei (Southern Italy). Journal of Volcanology and Geothermal Research, 133(1-4), 211-228.

Dellino, P., Isaia, R., La Volpe, L., & Orsi, G. (2004b). Interaction between particles transported by fallout and surge in the deposits of the Agnano–Monte Spina eruption (Campi Flegrei, Southern Italy). Journal of Volcanology and Geothermal Research, 133(1-4), 193-210.

Dietrich, P., Ghienne, J. F., Normandeau, A., & Lajeunesse, P. (2016). Upslope-migrating bedforms in a proglacial sandur delta: cyclic steps from river-derived underflows? Journal of Sedimentary Research, 86(1), 112-122.

Douillet, G. A., Tsang-Hin-Sun, È., Kueppers, U., Letort, J., Pacheco, D. A., Goldstein, F., Von Aulock, F., Lavallée, Y., Hanson, J. B., Bustillos, J., et al. (2013a) Sedimentology and geomorphology of the deposits from the August 2006 pyroclastic density currents at Tungurahua volcano, Ecuador, B. Volcanol., 75, 1–21

Douillet, G. A., Pacheco, D. A., Kueppers, U., Letort, J., Tsang-Hin-Sun, È., Bustillos, J., Hall, M., Ramón, P., and Dingwell, D.B. (2013b) Dune bedforms produced by dilute pyroclastic density currents from the August 2006 eruption of Tungurahua volcano, Ecuador, B. Volcanol., 75, 1–20,

Douillet, G.A., Rasmussen, K.R., Kueppers, U., Lo Castro, D., Merrison, J., Iversen, J., Dingwell, D.B. (2014) Saltation threshold for pyroclasts at various bedslopes: Wind tunnel measurements. J. Volc. Geotherm. Res. 278-279:14-24

Douillet, G.A. (2015) Flow and sedimentation from pyroclastic density currents. From large scale to boundary layer processes. PhD Dissertation, October 2014, Earth and Environmental Sciences, Ludwig Maximilian University, 2015

Douillet, G.A., Taisne, B., Tsang-Hin-Sun, E., Mueller, S.K., Kueppers, U., Dingwell, D.B. (2015) Syn-eruptive, soft-sediment deformation of dilute pyroclastic density current deposits: triggers from granular shear, dynamic pore pressure, ballistic impacts and shock waves. Solid Earth Discussion. http://www.solid- earth-discuss.net/6/3261/2014/sed-6-3261-2014.pdf

Douillet, G.A., Bouysson, M., Gegg, L. (2017) Overturned strata in deposits of dilute pyroclastic density currents, field and analogue data. IAVCEI general Assembly 2017 Portland, Oregon. Abstract

Douillet, G.A., Kueppers, U., Mato, C., Chaffaut, Q., Bouysson, M., Reschetizka, R., Hölscher, I., Witting, P., Hess, K.U., Cerwenka, A., Dingwell, D.B., Bernard, B. (in press) Revisiting the lacquer peels method with pyroclastic deposits: Sediment plates, a precise, fine-scale imaging method and powerful outreach tool. Journal of applied Volcanology

Douillet, G.A., Chaffaut, Q., Schlunegger, F., Kueppers, U., Dingwell, D.B. (submitted) Shark fin structures: overturned convolute and flame patterns due to waves at the shear horizon of a flow-bed boundary. Examples from the deposits of the 2006 pyroclastic currents at Tungurahua volcano (Ecuador). Sedimentology

Druitt, T.H. (1992) Emplacement of the 18 May 1980 lateral blast deposit ENE of Mount St. Helens, Washington. Bull Volcanol 54:554–572

Dufek, J. (2016). The fluid mechanics of pyroclastic density currents. Annual Review of Fluid Mechanics, 48, 459-485.

Dujardin, J. R. (2014). Imagerie géoradar (GPR) en milieu hétérogène: application aux failles actives en Mongolie et aux dépôts pyroclastiques du Tungurahua (Equateur) (Doctoral dissertation, Université de Strasbourg).

Dumas, S., Arnott, R. W. C., & Southard, J. B. (2005). Experiments on oscillatory-flow and combined-flow bed forms: implications for interpreting parts of the shallow-marine sedimentary record. Journal of Sedimentary research, 75(3), 501-513.

Fisher, R. V., & Waters, A. C. (1969). Bed forms in base-surge deposits: Lunar implications. Science, 165(3900), 1349-1352.

Fisher, R. V., & Waters, A. C. (1970). Base surge bed forms in maar volcanoes. American Journal of Science, 268(2), 157-180.

Fisher, R.V., 1977. Erosion by volcanic base-surge density currents; U-shaped channel. Geological Society of America Bulletin 88, 1287–1297.

Fisher, R. V., Schmincke, H. U., & Van Bogaard, P. (1983). Origin and emplacement of a pyroclastic flow and surge unit at Laacher See, Germany. Journal of volcanology and geothermal research, 17(1-4), 375-392.

Fisher, R. V. (1990). Transport and deposition of a pyroclastic surge across an area of high relief: the 18 May 1980 eruption of Mount St. Helens, Washington. Geological Society of America Bulletin, 102(8), 1038-1054.

Gençalioğlu-Kuşcu, G., Atilla, C., Cas, R. A., & Kuşcu, İ. (2007). Base surge deposits, eruption history, and depositional processes of a wet phreatomagmatic volcano in Central Anatolia (Cora Maar). Journal of Volcanology and Geothermal Research, 159(1-3), 198-209.

Ghienne, J. F., Girard, F., Moreau, J., & Rubino, J. L. (2010). Late Ordovician climbing-dune cross-stratification: a signature of outburst floods in proglacial outwash environments?. Sedimentology, 57(5), 1175-1198.

Giannetti, B., & Luongo, G. (1994). Trachyandesite scoria-flow and associated trachyte pyroclastic flow and surge at Roccamonfina Volcano (Roman Region, Italy). Journal of volcanology and geothermal research, 59(4), 313-334.

Hage, S., Cartigny, M. J., Clare, M. A., Sumner, E. J., Vendettuoli, D., Hughes Clarke, J. E., ... & Englert, R. G. (2018). How to recognize crescentic bedforms formed by supercritical turbidity currents in the geologic record: Insights from active submarine channels. Geology, 46(6), 563-566.

Hall, M. L., Steele, A. L., Mothes, P. A., & Ruiz, M. C. (2013). Pyroclastic density currents (PDC) of the 16–17 August 2006 eruptions of Tungurahua volcano, Ecuador: Geophysical registry and characteristics. Journal of Volcanology and Geothermal Research, 265, 78-93.

Hiscott, R. N. (1994). Loss of capacity, not competence, as the fundamental process governing deposition from turbidity currents. Journal of Sedimentary Research, 64(2).

Hoblitt, R. P. (1986). Observations of the eruptions of July 22 and August 7, 1980, at Mount St. Helens, Washington (No. 1335).

Jordan, S. C., Cas, R. A. F., & Hayman, P. C. (2013). The origin of a large (> 3 km) maar volcano by coalescence of multiple shallow craters: Lake Purrumbete maar, southeastern Australia. Journal of Volcanology and Geothermal Research, 254, 5-22.

Kelfoun, K., Samaniego, P., Palacios, P., & Barba, D. (2009). Testing the suitability of frictional behaviour for pyroclastic flow simulation by comparison with a well-constrained eruption at Tungurahua volcano (Ecuador). Bulletin of volcanology, 71(9), 1057.

Kennedy, J. F. (1963). The mechanics of dunes and antidunes in erodible-bed channels. Journal of Fluid mechanics, 16(4), 521-544.

Kieffer, S. W., & Sturtevant, B. (1988). Erosional furrows formed during the lateral blast at Mount St. Helens, May 18, 1980. Journal of Geophysical Research: Solid Earth, 93(B12), 14793-14816.

Kneller, B., & Buckee, C. (2000). The structure and fluid mechanics of turbidity currents: a review of some recent studies and their geological implications. *Sedimentology*, *47*(s1), 62-94.

Kubo, Y., & Nakajima, T. (2002). Laboratory experiments and numerical simulation of sediment-wave formation by turbidity currents. Marine Geology, 192(1-3), 105-121.

Leclair, S. F., & Arnott, R. W. C. (2005). Parallel lamination formed by high-density turbidity currents. Journal of Sedimentary Research, 75(1), 1-5.

Mattson, P. H., & Alvarez, W. (1973). Base surge deposits in Pleistocene volcanic ash near Rome. Bulletin Volcanologique, 37(4), 553-572.

Le Roux, J. P. (2005). Comments on "Turbulent boundary layer shear flows as an approximation of base surges at Campi Flegrei (Southern Italy), by Dellino et al.(2004)". Journal of Volcanology and Geothermal Research, 141(3-4), 331-332.

Nakajima, T., & Satoh, M. (2001). The formation of large mudwaves by turbidity currents on the levees of the Toyama deep-sea channel, Japan Sea. Sedimentology, 48(2), 435-463.

Palladino, D. M. (2017). Simply pyroclastic currents. Bulletin of Volcanology, 79(7), 53.

Ponce, J. J., & Carmona, N. (2011). Coarse-grained sediment waves in hyperpycnal clinoform systems, Miocene of the Austral foreland basin, Argentina. Geology, 39(8), 763-766.

Richards, A.F., 1959. Geology of the Islas Revillagigedo, Mexico. 1, birth and development of Volcan Barcena, Isla San Benedicto (1). Bulletin of Volcanology 22, 73–123.

Rowley, P. J., Roche, O., Druitt, T. H., & Cas, R. (2014). Experimental study of dense pyroclastic density currents using sustained, gas-fluidized granular flows. Bulletin of Volcanology, 76(9), 855.

Schmincke, H. U., Fisher, R. V., & Waters, A. C. (1973). Antidune and chute and pool structures in the base surge deposits of the Laacher See area, Germany. Sedimentology, 20(4), 553-574.

Simpson, J. E. (1982). Gravity currents in the laboratory, atmosphere, and ocean. Annual Review of Fluid Mechanics, 14(1), 213-234.

Sohn, Y. K., & Chough, S. K. (1989). Depositional processes of the Suwolbong tuff ring, Cheju Island (Korea). Sedimentology, 36(5), 837-855.

Sparks, R. S. J., & Walker, G. P. L. (1973). The ground surge deposit: a third type of pyroclastic rock. Nature physical science, 241(107), 62.

Spinewine, B., Sequeiros, O. E., Garcia, M. H., Beaubouef, R. T., Sun, T., Savoye, B., & Parker, G. (2009). Experiments on wedge-shaped deep sea sedimentary deposits in minibasins and/or on channel levees emplaced by turbidity currents. Part II. Morphodynamic evolution of the wedge and of the associated bedforms. Journal of Sedimentary Research, 79(8), 608-628.

Sulpizio, R., Mele, D., Dellino, P., & La Volpe, L. (2007). Deposits and physical properties of pyroclastic density currents during complex Subplinian eruptions: the AD 472 (Pollena) eruption of Somma-Vesuvius, Italy. Sedimentology, 54(3), 607-635.

Sulpizio, R., Dellino, P., Doronzo, D. M., & Sarocchi, D. (2014). Pyroclastic density currents: state of the art and perspectives. Journal of Volcanology and Geothermal Research, 283, 36-65.

Suthren, R. J. (1985). Facies analysis of volcaniclastic sediments: a review. Geological Society, London, Special Publications, 18(1), 123-146.

Vallis, G.K., 2006. Atmospheric and Oceanic Fluid Dynamics—Fundamentals and Large Scale Circulation. Cambridge University Press (ISBN: 978-0-521-84969-2).

Vellinga, A. J., Cartigny, M. J., Eggenhuisen, J. T., & Hansen, E. W. (2018). Morphodynamics and depositional signature of low-aggradation cyclic steps: New insights from a depth-resolved numerical model. Sedimentology, 65(2), 540-560.

Viroulet, S., Baker, J. L., Edwards, A. N., Johnson, C. G., Gjaltema, C., Clavel, P., & Gray, J. M. N. T. (2017). Multiple solutions for granular flow over a smooth two-dimensional bump. Journal of Fluid Mechanics, 815, 77-116.

Walker, G. P. L., Wilson, C. J. N., & Froggatt, P. C. (1981). An ignimbrite veneer deposit: the trail-marker of a pyroclastic flow. Journal of Volcanology and Geothermal Research, 9(4), 409-421.

Walker, G. P. (1984). Characteristics of dune-bedded pyroclastic surge bedsets. Journal of Volcanology and Geothermal Research, 20(3-4), 281-296.

Waters, A. C., & Fisher, R. V. (1971). Base surges and their deposits: Capelinhos and Taal volcanoes. Journal of Geophysical Research, 76(23), 5596-5614.

Wohletz, K. H., & Sheridan, M. F. (1979). A model of pyroclastic surge. Geol Soc Am Spec Pap, 180, 177-194.

Yokoyama, S., & Tokunaga, T. (1978). Base-surge deposits of Mukaiyama volcano, Nii-jima, Izu Islands. Bull Volcanol Soc Jpn, 23, 249-262.

Zedler, E. A., & Street, R. L. (2001). Large-eddy simulation of sediment transport: currents over ripples. Journal of Hydraulic Engineering, 127(6), 444-452.

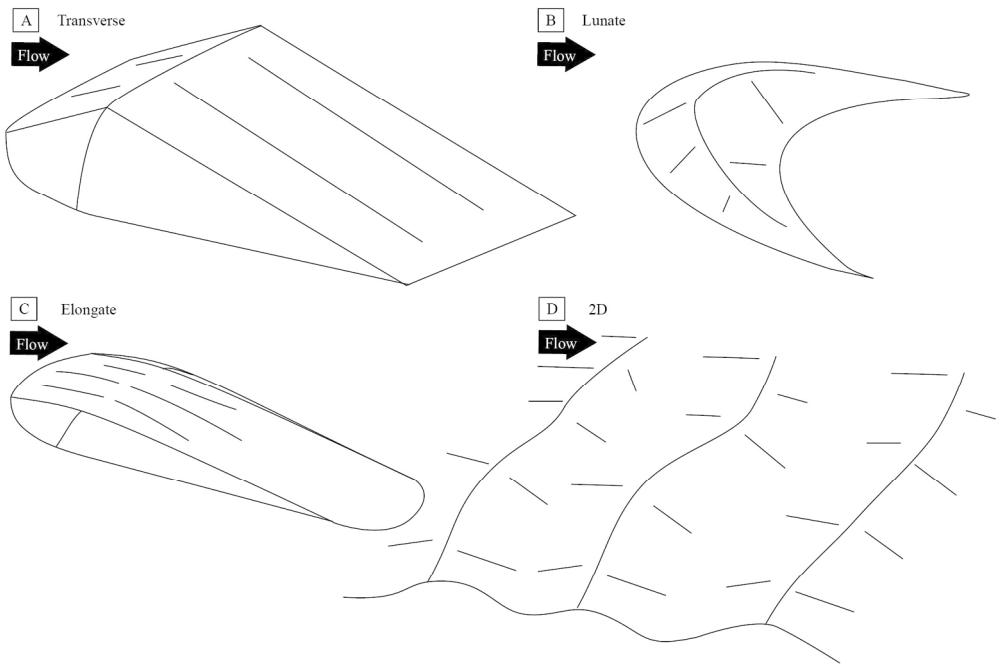

Figure 1: Sketch of the four different bedform shapes identified at Tungurahua. A: Transverse, B: Lunate, C: Elongate, D: 2D.

180x119mm (300 x 300 DPI)

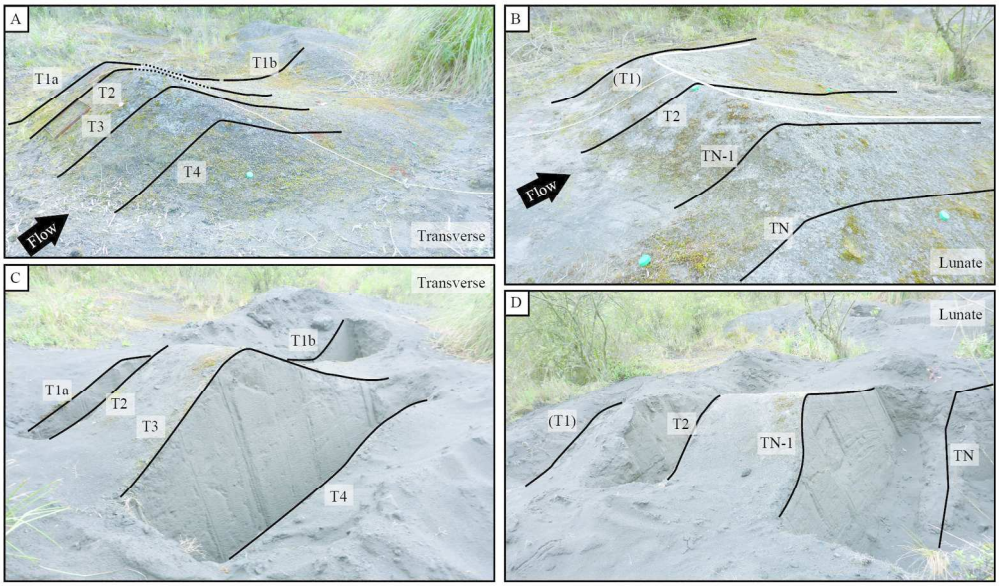

Figure 2: Surface shape (A resp. B), and the trenches realized to impregnate the transects (C resp. D) for the of the transverse resp. lunate bedform.

180x105mm (300 x 300 DPI)

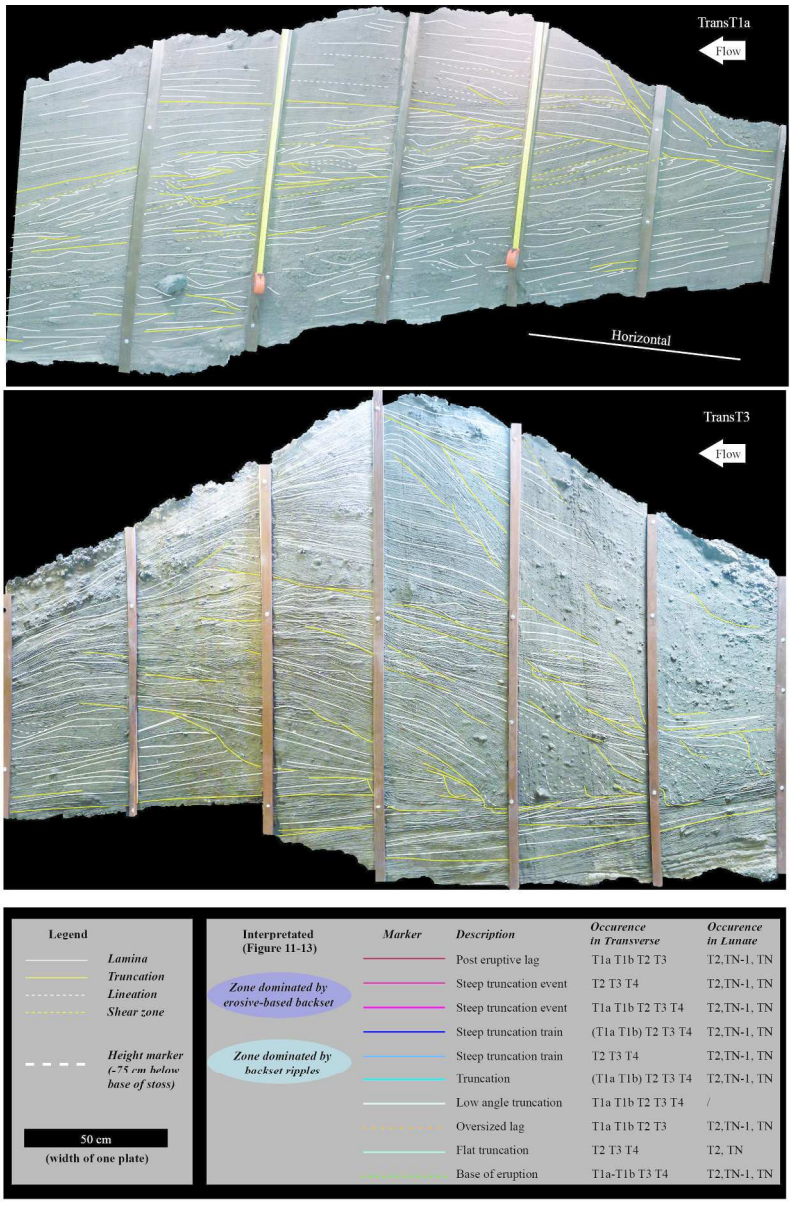

Figure 3: Transects within the Transverse bedform. Flow toward the center of the book. All transects are formed by 6 individual plates 50 cm broad, forming a 3 m long profile. Transect T1a and T1b connect to form a 6 m long profile.

180x272mm (300 x 300 DPI)

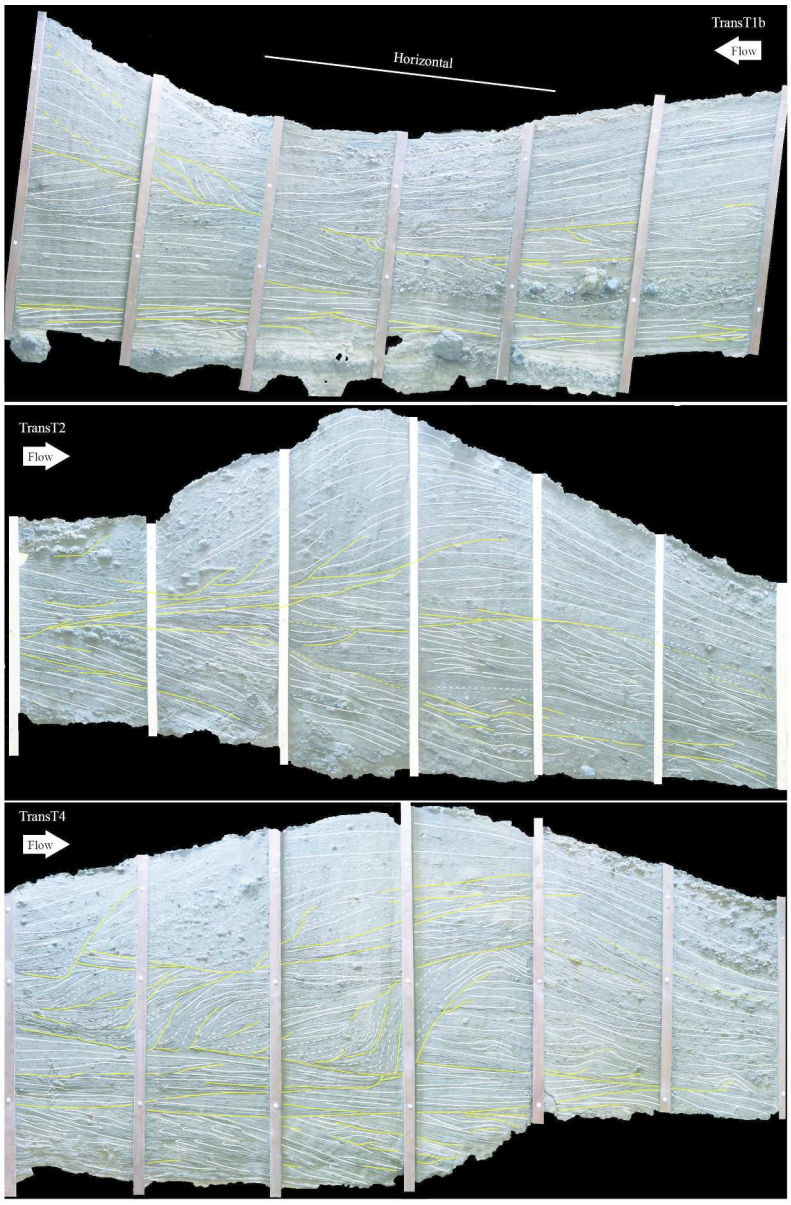

second part of figure 3

180x272mm (300 x 300 DPI)

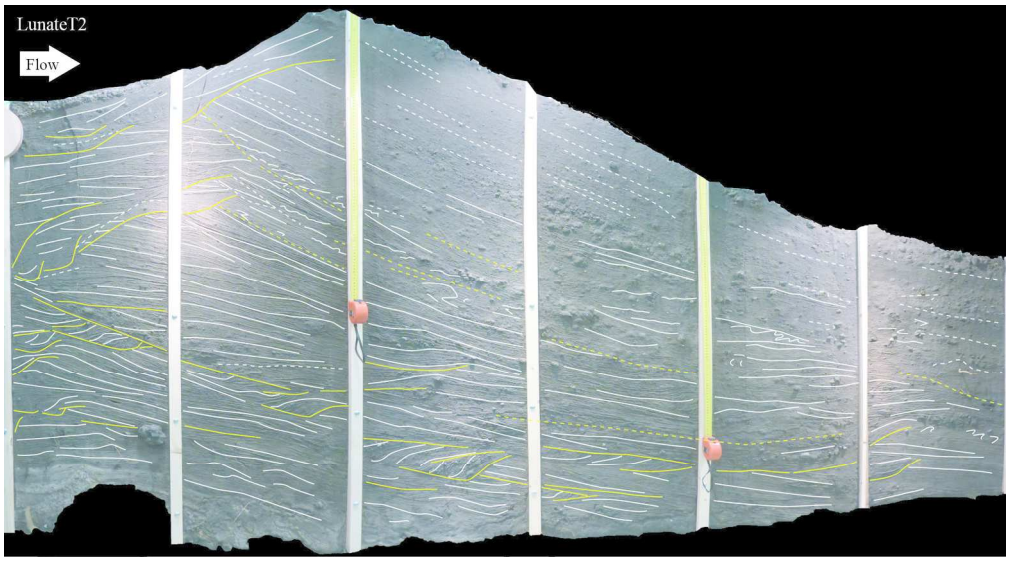

Figure 4A: Transects within the lunate bedform. Flow toward the center of the book. All transects are formed by 6 individual plates 50 cm broad, forming a 3 m long profile.

176x97mm (300 x 300 DPI)

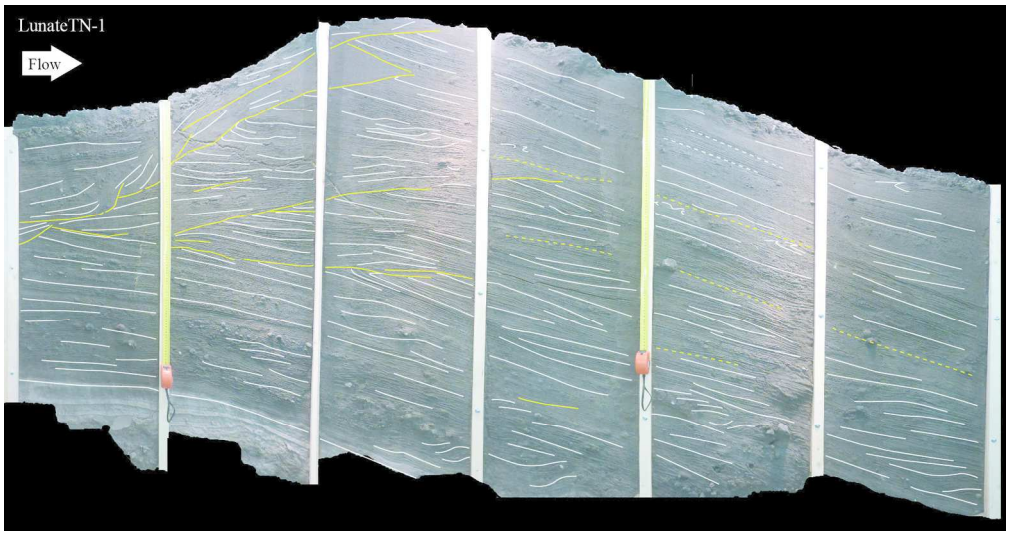

Figure 4B: second part of lunate transects

177x93mm (300 x 300 DPI)

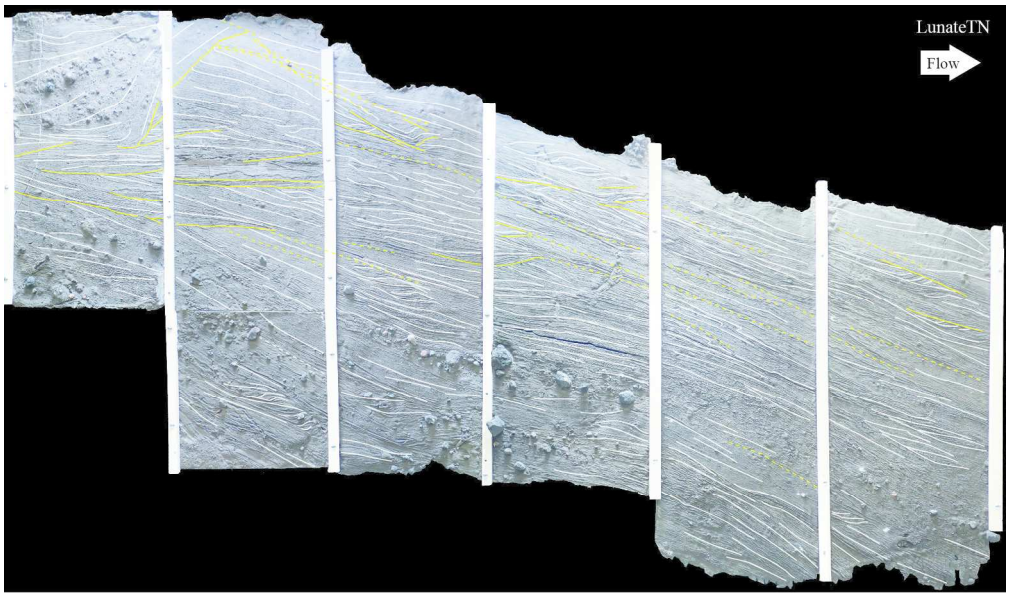

Figure 4C: third part of lunate transects

177x104mm (300 x 300 DPI)

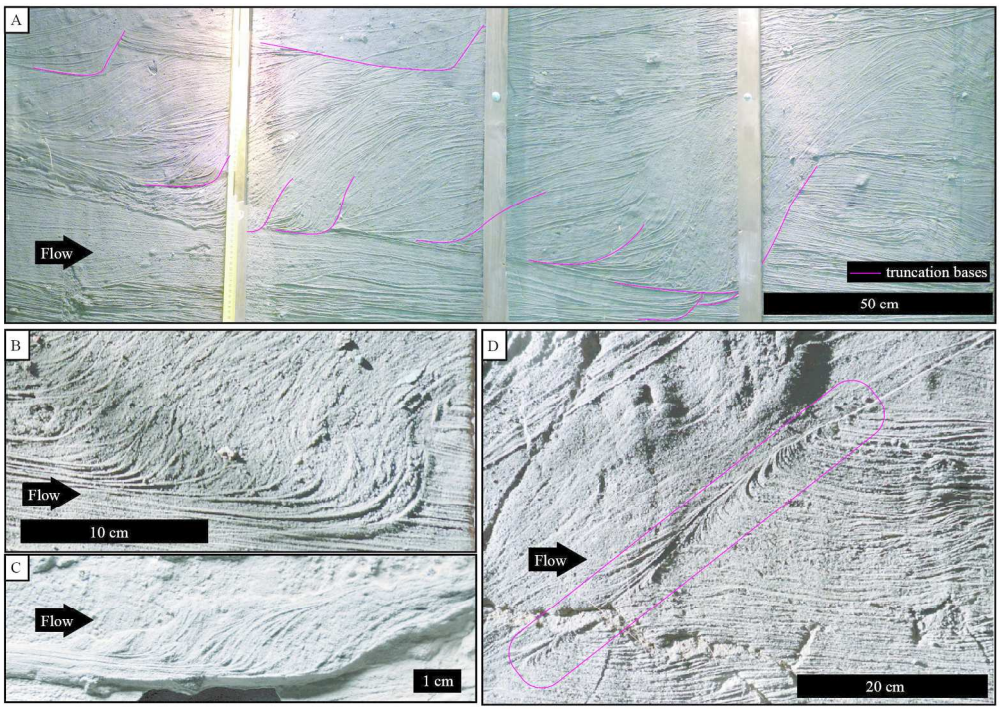

Stoss-side features. A-C: Erosive-based backset trains at different scales, A: Bedform scale (Trans-T4P1-4), B: Vertical truncation with vertical and overhanging infill of backset lineations (Trans-T3P1)., C: Small-scale erosive-based backsets in silt-sized ash. D: Truncation with overturned lamination (Luna-T3P2).

180x127mm (300 x 300 DPI)

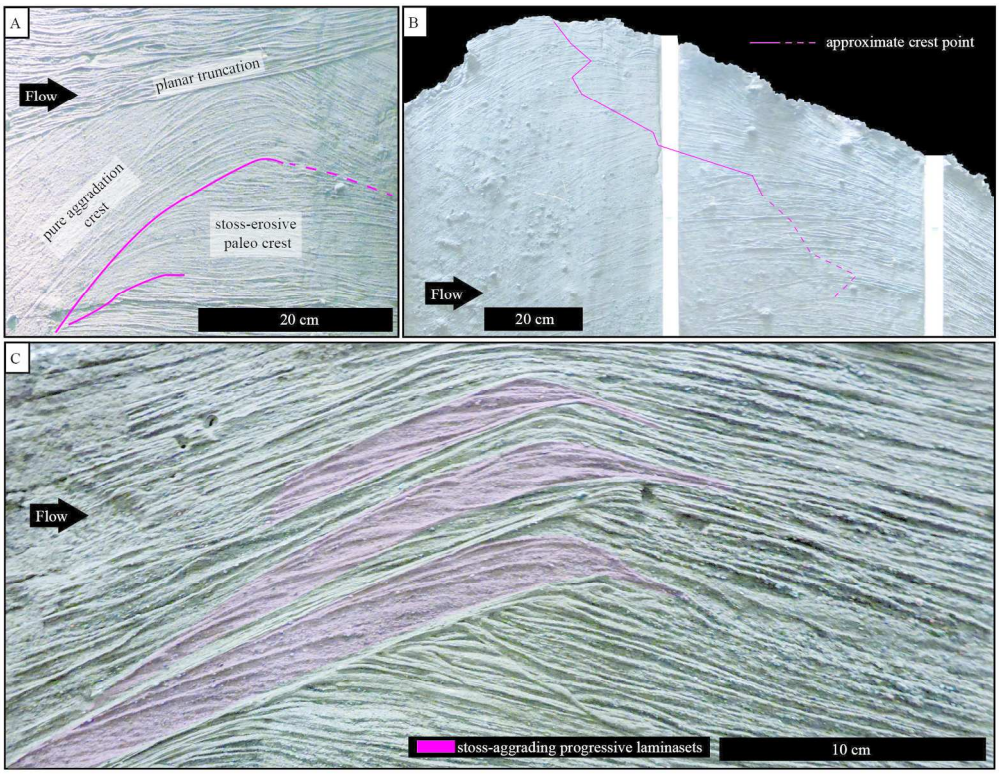

Figure 6: Crest features. A: Pure-aggradation crest bedset building on a stoss-erosive paleo crest and subsequently cut by planar truncation (Trans-T4P4). B: Pure-aggradation crest with upstream preferential deposition in the terminal sedimentation phase of growth (Trans-T2P3-4). C: Regressive (stoss-depositional) beds containing prograding laminasets. Note that laminaset vanish as soon as the paleo-crest is reached (Plate from a previously investigated transverse bedform presented in Douillet et al. 2015).

180x139mm (300 x 300 DPI)

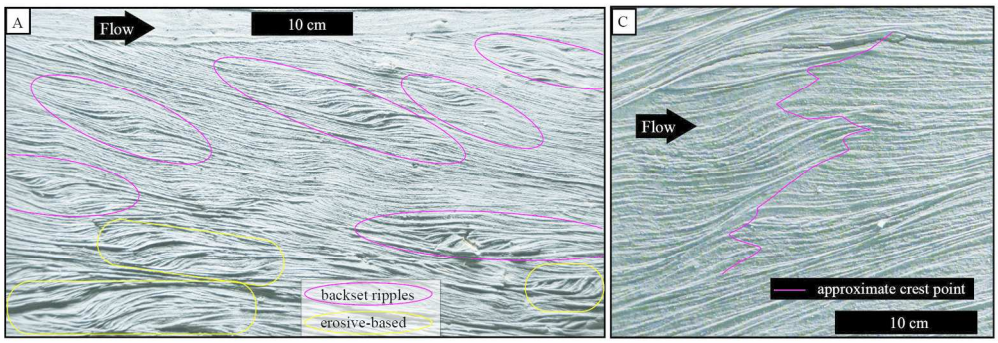

Backset ripples. A: Patches of backset ripples and erosive-based backset trains (Trans-T4P1). B: Propagation of a backset ripple structure through the stratigraphy, with evolving behavior from preferential stoss- or lee-deposition (regressive and progressive, TransT3P4). The pink line follows the successive position of the crest.

180x61mm (300 x 300 DPI)

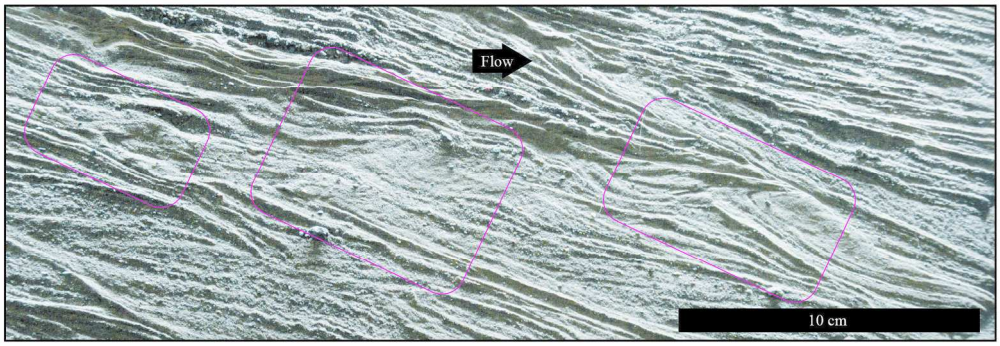

Figure 8: Train of three shark fin structures interpreted as representing shear instabilities at the base of the flow (see Douillet et al. this issue).

180x61mm (300 x 300 DPI)

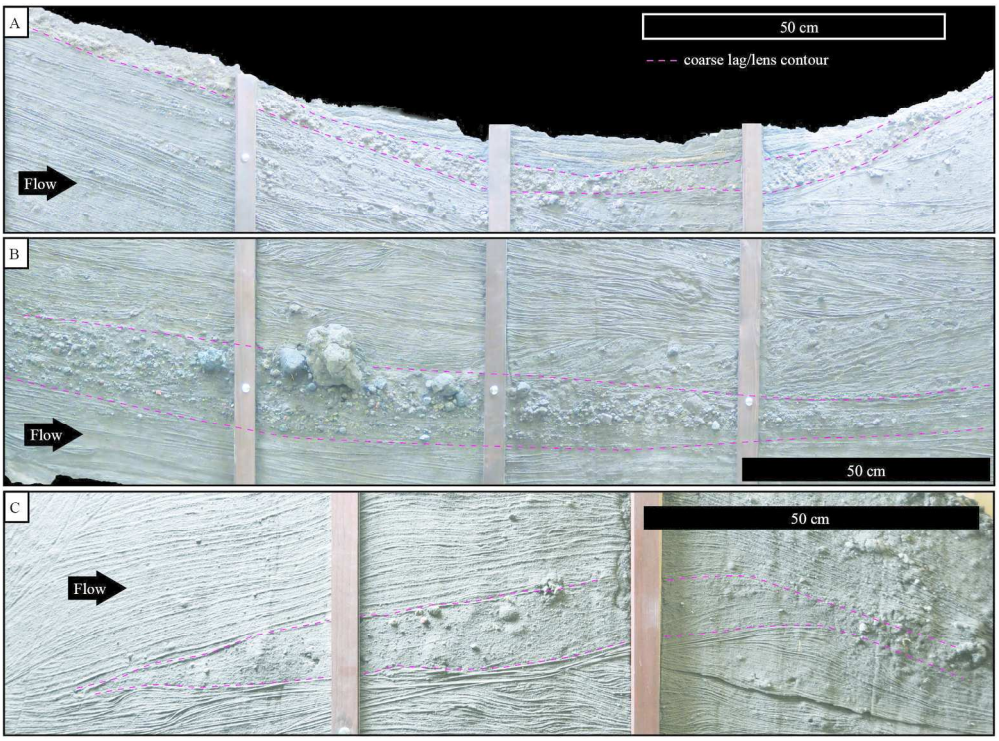

Figure 9: Coarse-grained lags and lenses. A: Superficial lag formed of light gray pumice (Trans-T1bP3-6). B: Horizon with oversized clasts that vanish laterally into finer grained particles and eventually disappears (Trans-T1bP1-4). C: Relatively coarse and massive lens that forms on the stoss side of a paleo-crest and vanishes on the lee (Trans-T3P3-5).

180x132mm (300 x 300 DPI)

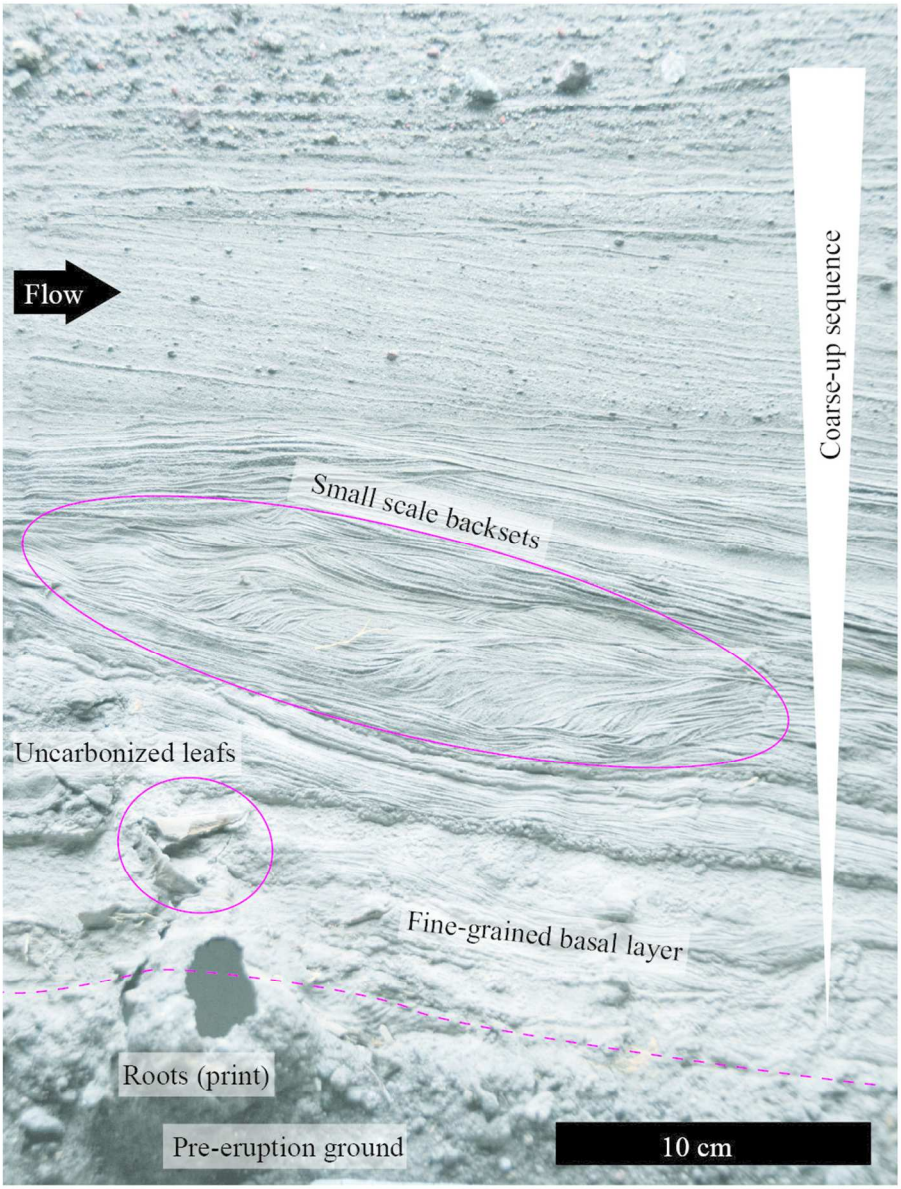

Figure 10: Basal contact of the 2006 eruption (Trans-T1bP4). Note the coarse and weathered ground overlain by silt-sized ash beds containing uncarbonized orchid leafs (Epidendrum Jamiesonis) and fine scale erosive-based backset structures. The sequence is sharply coarsening-up.

90x118mm (300 x 300 DPI)

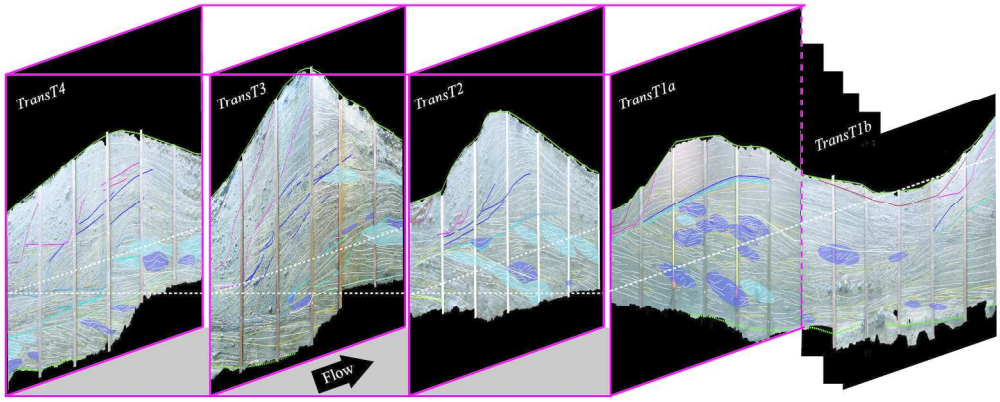

Figure 11: A possible correlation of the Transverse transects. Truncations are highlighted with colors that relate to the same bursts on the different transects.

180x74mm (300 x 300 DPI)

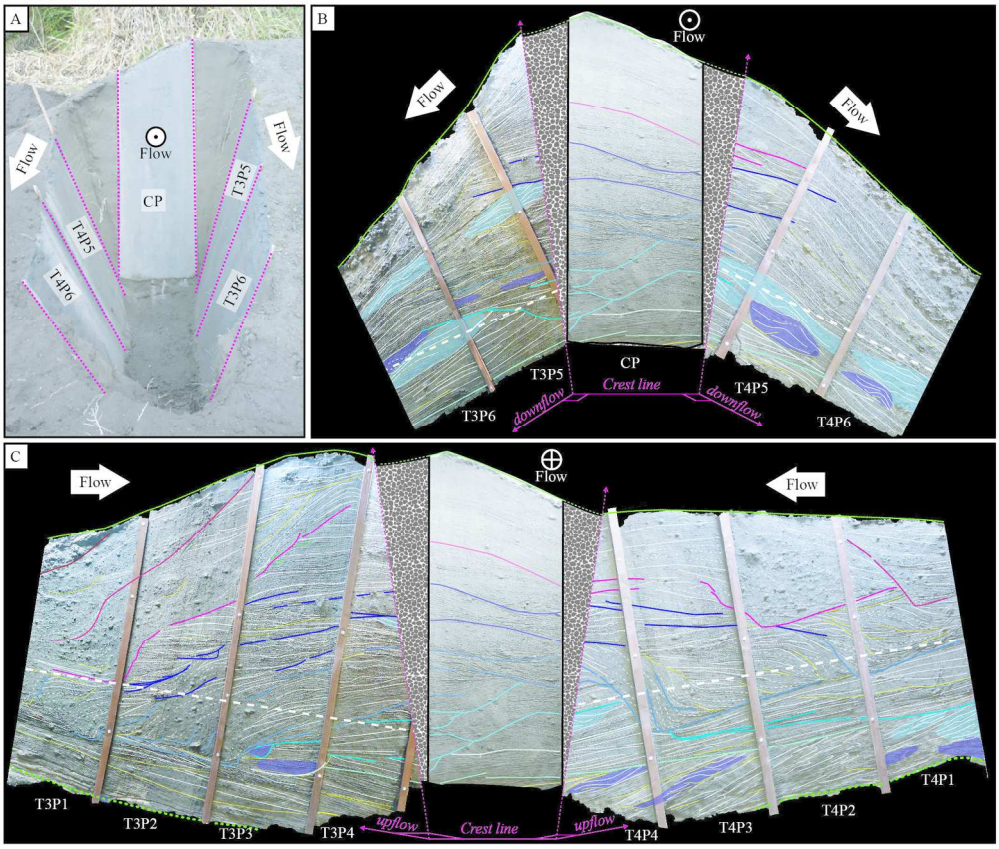

Figure 12: Cross profile between Trans T3 and Trans T4. A) Plate organization in the field. B) Interpreted relations in the downstream direction.C) Interpreted relations in the upstream direction.

180x152mm (300 x 300 DPI)

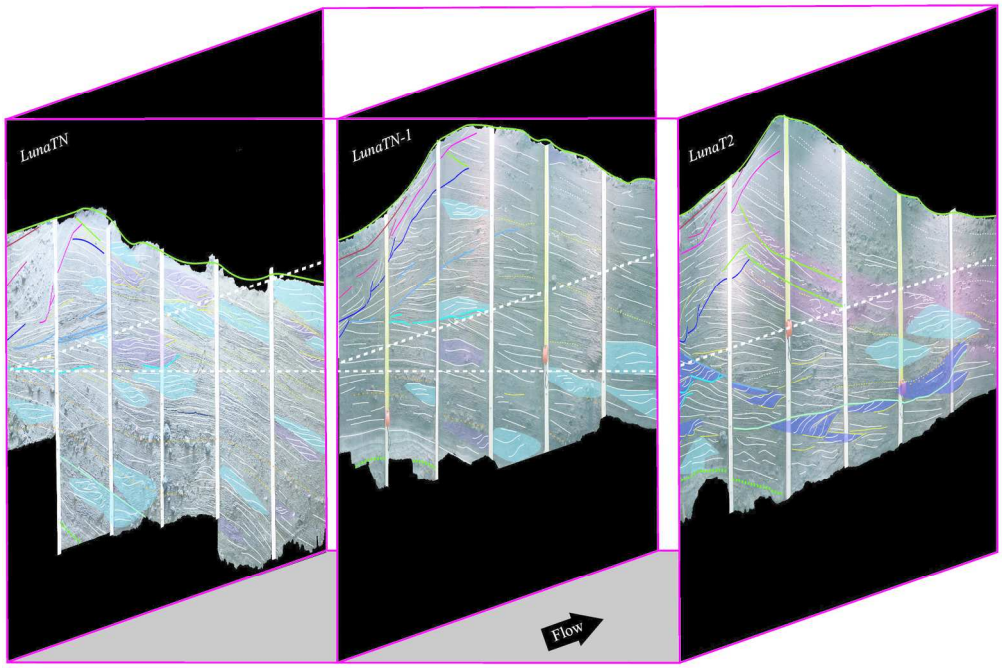

Figure 13: A possible correlation of the Lunate transects. The color coding is based on the same events as for the transverse bedform (these two structures are separated by ca. 10 m in the field).

180x121mm (300 x 300 DPI)

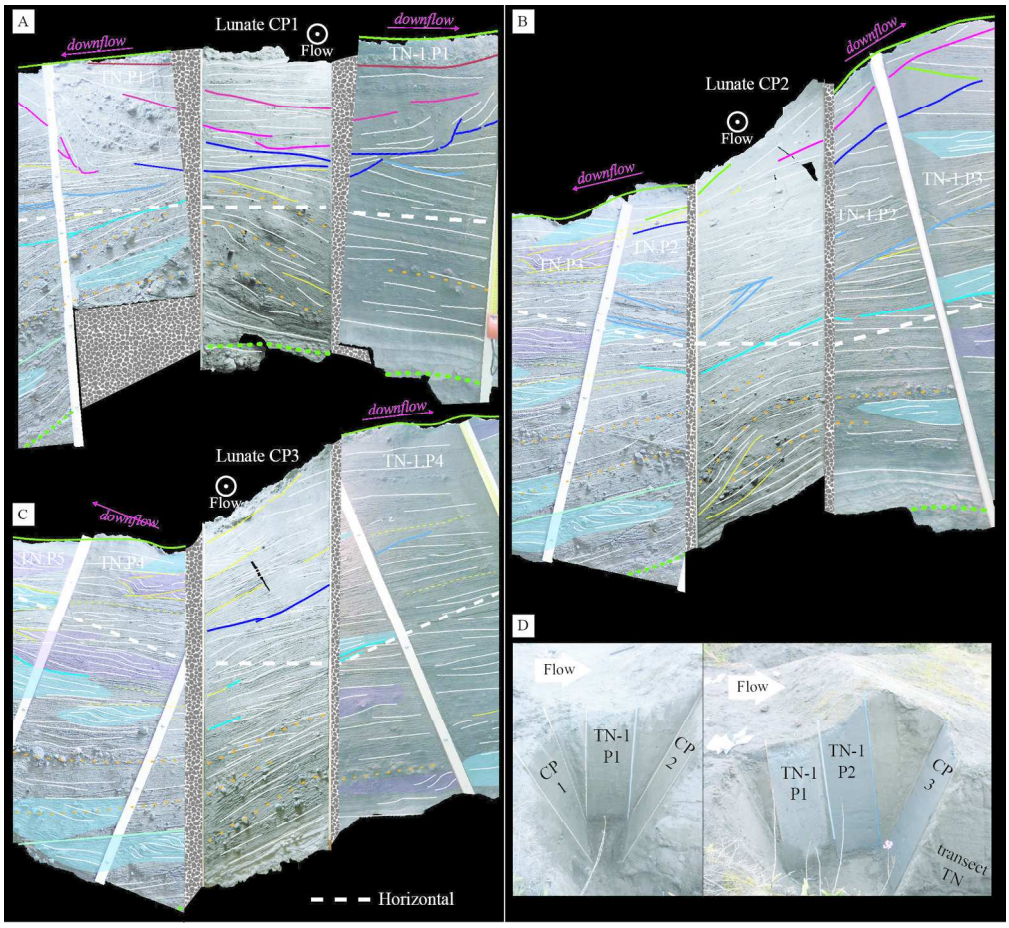

Figure 14: Cross profiles (CP) between Lunate TN-1 and Lunate TN. A) CP1: upstream toe of bedform B) CP2: above the crest, C) CP3: on the lee-side. D) Plate organization in the field.

180x165mm (300 x 300 DPI)

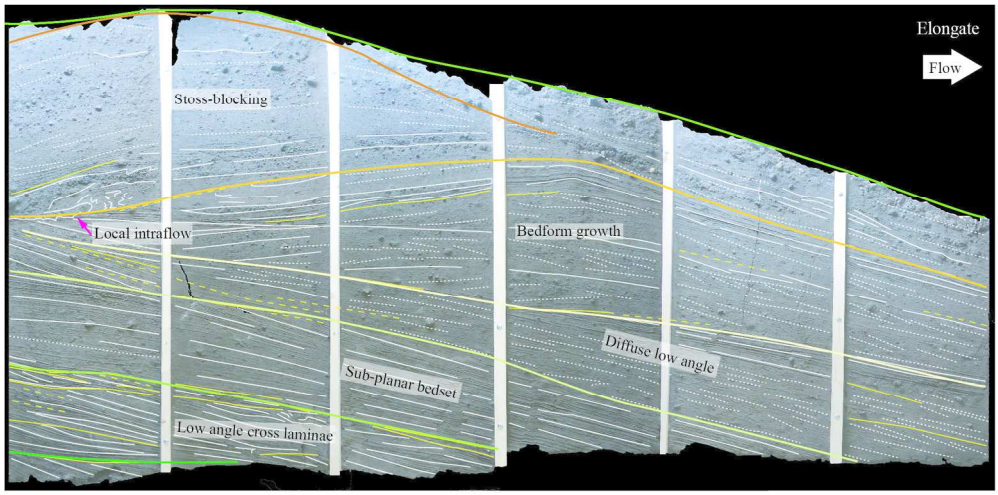

Figure 15: Interpreted transect of the Elongate bedform. This bedform is the most proximal, situated ca. 2 km up-valley from the transverse and lunate outcrops. For details on the massive lens and deformed beds, see Douillet et al. this issue.

180x88mm (300 x 300 DPI)

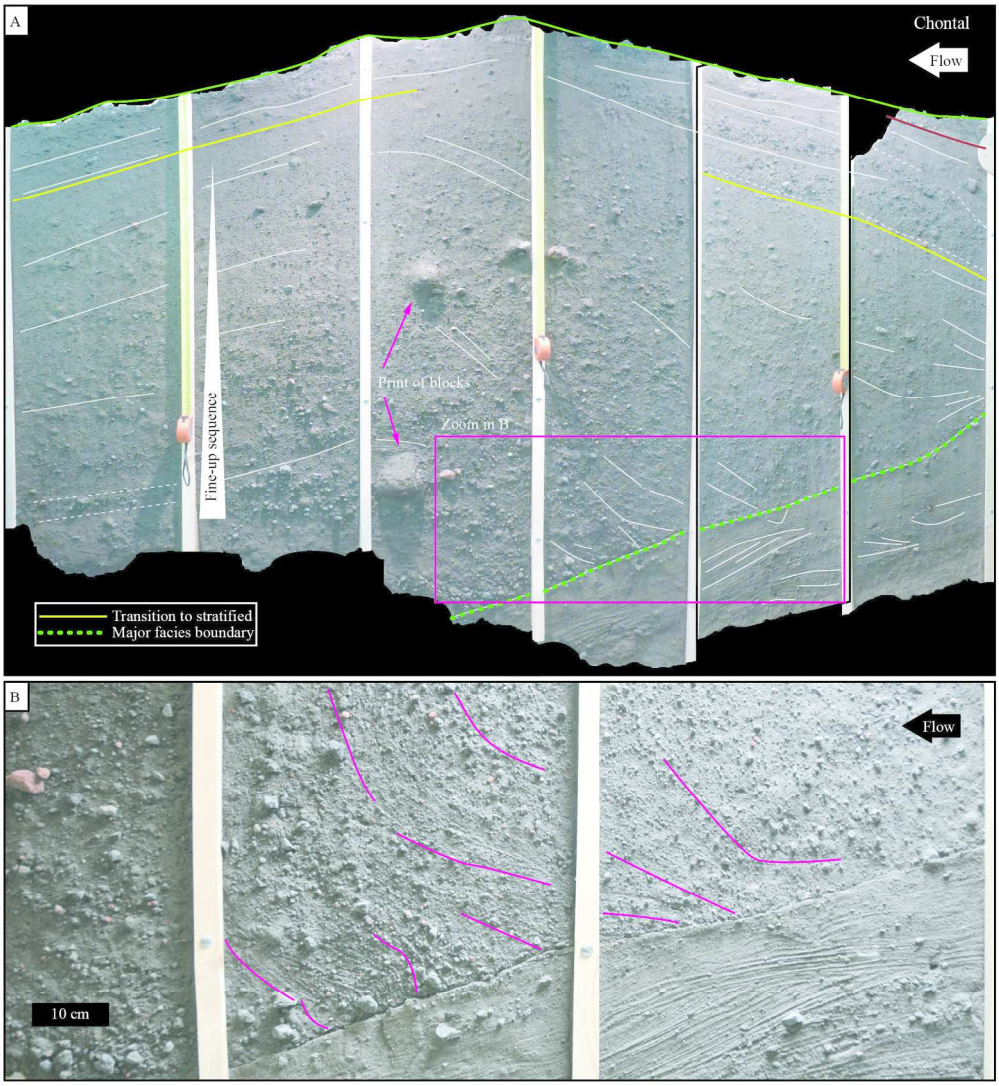

Figure 16: A) Interpreted transect of the bedform from the Chontal area. B) Zoom of the zone highlighted in A reveals the coarse-lineated facies and contact with lowermost unit.

180x196mm (300 x 300 DPI)

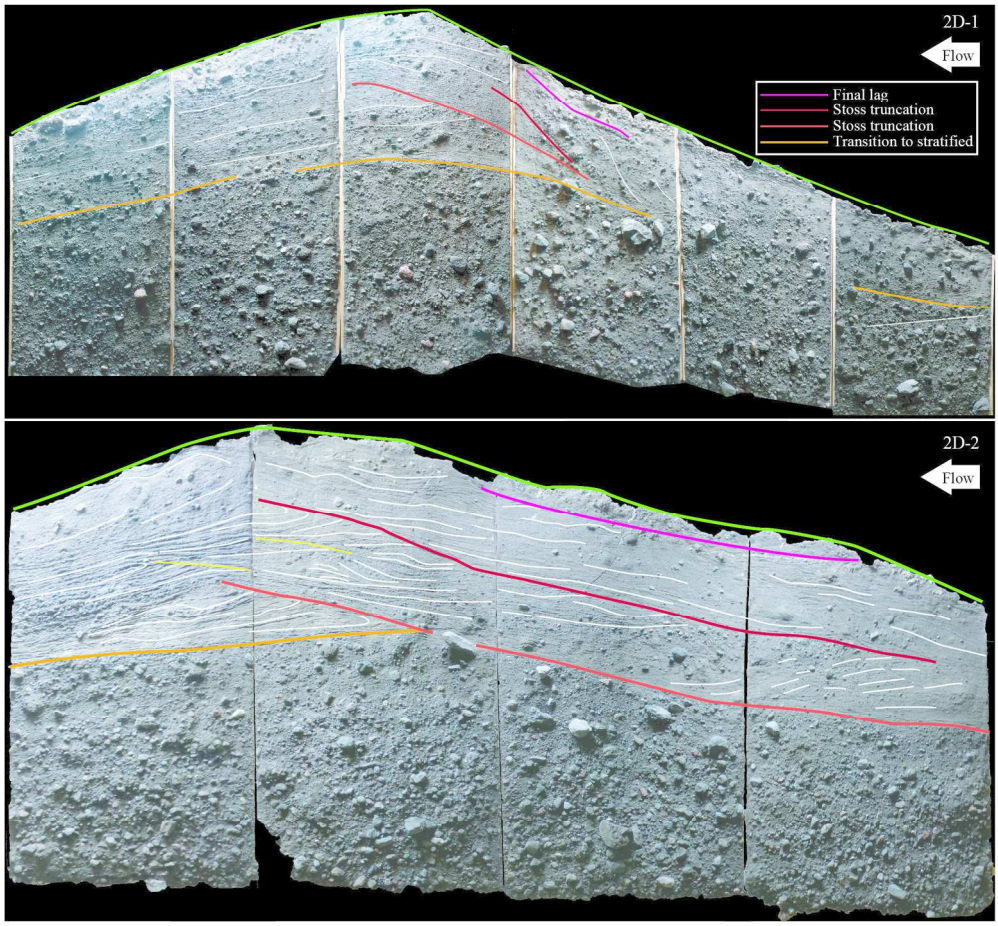

Figure 17: Interpreted transects from the 2D bedforms. These are located in the most distal deposits, situated ca. 500 m down-valley from the transverse and lunate bedforms.

180x166mm (300 x 300 DPI)

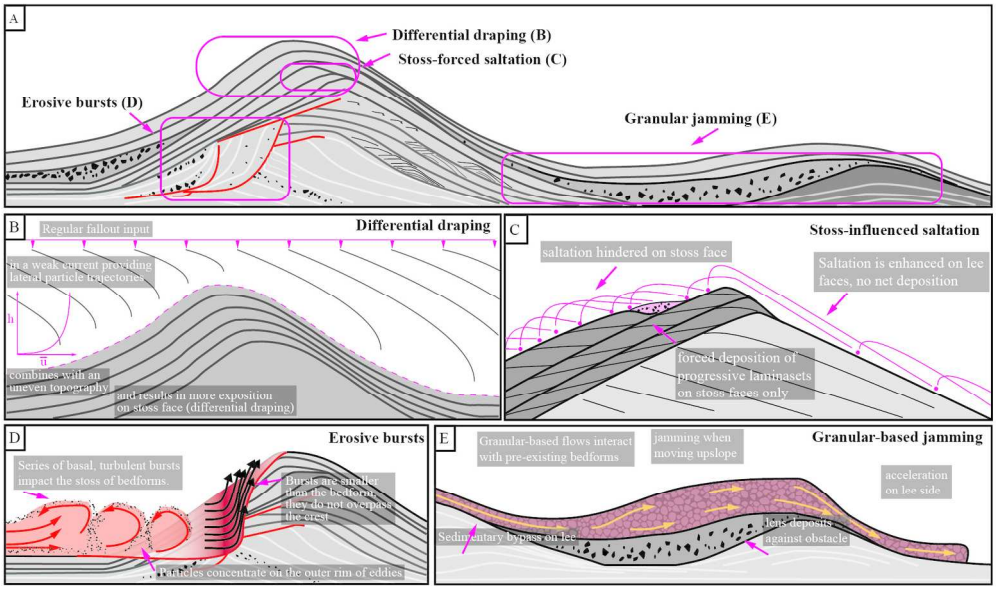

Figure 18: Interpretative sketch of the four formational mechanisms for pyroclastic bedforms. A) General sketch of a bedform, B) Differential draping, C) Stoss-influenced saltation D) Erosive basal bursts, E) Granular jamming.

180x106mm (300 x 300 DPI)